

# Phoretic Motion of Spheroidal Particles Due To Self-Generated Solute Gradients

M. N. Popescu<sup>1</sup>, S. Dietrich<sup>2,3</sup>, M. Tasinkevych<sup>2,3</sup>, and J. Ralston<sup>1</sup>

<sup>1</sup> Ian Wark Research Institute, University of South Australia, 5095 Adelaide, South Australia, Australia

e-mail: Mihail.Popescu@unisa.edu.au

e-mail: John.Ralston@unisa.edu.au

<sup>2</sup> Max-Planck-Institut für Metallforschung, Heisenbergstr. 3, 70569 Stuttgart, Germany

<sup>3</sup> Institut für Theoretische und Angewandte Physik, Universität Stuttgart, Pfaffenwaldring 57, 70569 Stuttgart, Germany

e-mail: dietrich@mf.mpg.de

e-mail: miko@mf.mpg.de

Received: date / Revised version: date

**Abstract.** We study theoretically the phoretic motion of a spheroidal particle, which generates solute gradients in the surrounding unbounded solvent via chemical reactions active on its surface in a cap-like region centered at one of the poles of the particle. We derive, within the constraints of the mapping to classical diffusio-phoresis, an analytical expression for the phoretic velocity of such an object. This allows us to analyze in detail the dependence of the velocity on the aspect ratio of the polar and the equatorial diameters of the particle and on the fraction of the particle surface contributing to the chemical reaction. The particular cases of a sphere and of an approximation for a needle-like particle, which are the most common shapes employed in experimental realizations of such self-propelled objects, are obtained from the general solution in the limits that the aspect ratio approaches one or becomes very large, respectively.

PACS numbers: 89.20.-a, 82.70.Dd, 07.10.Cm

**PACS.** XX.XX.XX No PACS code given

## 1 Introduction

The increasing interest in the development of “lab on a chip” devices and of drug-delivery systems has led to a stringent need of scaling standard machinery down to micro- and nano-scales. This reduction in length scale has raised a number of challenging issues, such as developing ways to enable small objects to perform autonomous, directional motion [1,2].

Although the experimental and theoretical research in this area is still in its early stages, several proposals for such “self-propellers” have already been tested experimentally (see, e.g., Refs. [1,2,3,4,5]); a review of the recent progress in this field can be found in Ref. [6]. These “proof of principle” proposals have generally employed particles with axial symmetry, i.e., cylindrical rods [1,2] or spheres [4,5], because they are relatively easy to manufacture, allow for a good control of the desired surface modifications, and their simple geometry is a significant bonus for the theoretical analysis of the experimental results. The underlying idea, as put forward by Whitesides and co-workers [1], is that an asymmetric decoration of the

particle with a catalyst, which promotes an activated reaction in the surrounding liquid medium generating product molecules, can provide motility through a variety of mechanisms. As in the initial design proposed in Ref. [1], the simplest example is the propulsion of mm-size objects due to the ejection and subsequent bursting of bubbles formed by the product molecules [O<sub>2</sub> for PDMS plates with Pt catalyst tails placed in hydrogen peroxide (H<sub>2</sub>O<sub>2</sub>) aqueous solutions]. As the size of the particle is decreased towards the micron scale or below, viscous and surface forces start to dominate and inertia-based mechanisms such as the “bubble ejection” propulsion become ineffective. If the product molecules remain dissolved in the surrounding liquid medium as, e.g., in the experiments reported in Refs. [2,4,5], the result of an asymmetric distribution of catalyst is that the chemical reaction gives rise to concentration gradients along the surface of the particle. It has therefore been argued [2,7] that in such cases the motion of the catalyst-covered “active” particle is rather phoretic, i.e., the result of the interactions between the particle and the non-uniformly distributed product molecules generated by the chemical reaction. For example, in the case of Au-Pt rods in H<sub>2</sub>O<sub>2</sub>-H<sub>2</sub>O mixtures [2] the product molecules O<sub>2</sub> play the role of a solute the concentration gradient of

---

Correspondence to: M. N. Popescu

which in the solution (formed by the  $\text{H}_2\text{O}_2 - \text{H}_2\text{O}$  mixture as the solvent and  $\text{O}_2$  as the solute) is the field that may induce phoretic motion.

In many cases the magnitude and the direction of the experimentally observed phoretic velocity of such “active” particles are compatible with a variety of microscopic mechanisms, such as surface tension gradients [2,3,8] (note that Ref. [3] provides an elegant example that rotational motion can also be achieved), cyclic adsorption and desorption [6], electrokinetics [2,5,6,9], or diffusio-phoresis [4,7,10,11]. (By using the notion of diffusio-phoresis, here we refer strictly to phoresis due to gradients of a solute, i.e., we do not consider the case of bimetallic particles [2,6] for which charge transfer and electro-chemistry may be the dominant effects. For simplicity, we focus here on the case of electrically neutral solutes, which in the literature is often also called “chemo-phoresis”.) Thus understanding these systems and discriminating between these various possibilities require a careful, detailed theoretical analysis to predict the dependence of the velocity on the control parameters of the system, such as, e.g., the  $\text{H}_2\text{O}_2$  content of the aqueous hydrogen peroxide solvent used in the experiments reported in Refs. [2,4,5] or the fraction of the particle surface which is catalytically active. With the notable exception of Ref. [10], which has used a microscopic description for the interfacial region at the expense of having to carry out numerically most of the analysis, the theoretical approach so far has been to map these systems onto the case of classic phoresis in an *externally* imposed gradient of a field such as, e.g., a solute concentration or an electric potential (see Ref. [12] for a review of the theory of classic phoresis and additional references; a detailed discussion of the shortcomings of such a mapping is provided in Ref. [13]).

Starting from the model system proposed in Refs. [2,7], here we study the phoretic motion of a spheroidal particle which generates number density gradients of product molecules emerging from chemical reactions, which are active on the surface of the particle in a cap-like region centered at one of the poles. The product molecules diffuse into the surrounding unbounded three-dimensional Newtonian liquid solvent. Similar to the earlier studies in Refs. [7,11,13,14], our work is based on adopting the standard theory of phoresis for the present case, in which the gradients are self-generated rather than being produced and maintained by external sources [15]. The motivation for this work is to provide a unified description (within the standard theory) for the diffusio-phoretic motion of objects belonging to an extended class of geometrical shapes relevant to experimental studies [2,4,5,16]. The previously studied spherical and needle-like shaped objects are recovered as particular limiting cases. We note that here we focus on the case of rigid particles. If the body is actually soft and deformable various additional phenomena, such as a transfer between translational and rotational motion upon shape changes, may occur (see, e.g., Ref. [17]).

The outline of the paper is as follows. In Section 2 we define the model. Section 3 is devoted to the derivation of the diffusio-phoretic velocity; it includes also the compu-

tation of the distribution of the product molecules which induces the phoretic motion. The results, as well as the connections with the previous studies in Refs. [2,7,11,8], are discussed in Sec. 4. We conclude with a brief summary in Section 5.

## 2 The Model

The system we consider is shown in Fig. 1(a). It consists of an impermeable, spheroidal, rigid particle of polar and equatorial semi-axes  $R_1$  and  $R_2$ , respectively. At one of the poles there is a cap-like region (the black area in Fig. 1) covered by a catalyst [with density  $\sigma$  (number of catalytically active sites/unit area)] which promotes the chemical conversion of a surrounding solvent (not shown in Fig. 1) into product molecules of diameter  $a$  [small hatched circles in Fig. 1(a)]. (This is a so-called “Janus particle”[11].)

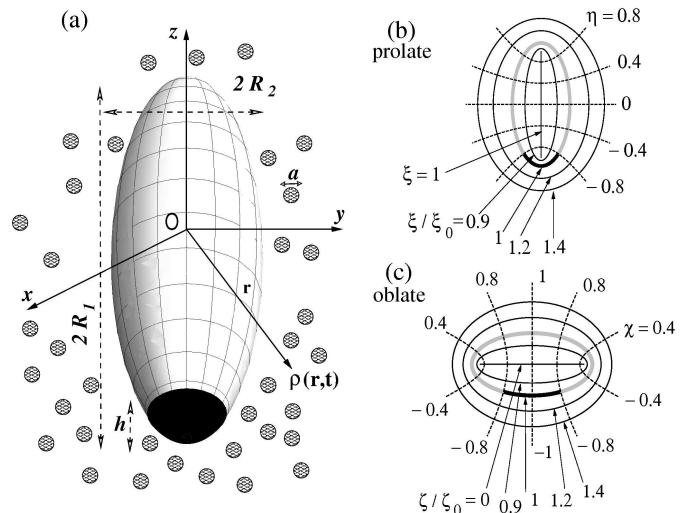


**Fig. 1.** (a) An impermeable, spheroidal particle of polar and equatorial semi-axes  $R_1$  and  $R_2$ , respectively, with a cap-like part of the surface covered by a catalyst (depicted as a black area). The aspect ratio of the particle is  $s_r = R_2/R_1$ ;  $s_r < 1$  (shown here) corresponds to a prolate shape, while  $s_r > 1$  to an oblate one.  $s_r = 1$  corresponds to a sphere. The product molecules of diameter  $a$  are shown as small hatched circles.  $O$  denotes the geometric center of the particle from which the number density  $\rho(\mathbf{r}, t)$  of product molecules is measured. (b) and (c) show cuts of the  $xz$  plane through the prolate and oblate iso-surfaces in terms of prolate  $(\xi, \phi, \eta)$  and oblate  $(\zeta, \phi, \chi)$  spheroidal coordinates, respectively [see, c.f., Eqs. (7)-(12) and Eqs. (20)-(24), respectively].  $\xi_0$  and  $\zeta_0$  denote the values of the prolate  $\xi$  and oblate  $\zeta$  coordinates, respectively, for which the corresponding iso-surfaces coincide with the surface of the particle (shown as a thick gray line; the thick black line at the lower pole indicates the catalyst covered region).

The shape of the object is characterized by its aspect ratio  $s_r = R_2/R_1$ :  $s_r < 1$  refers to a prolate spheroid,  $s_r > 1$  refers to an oblate spheroid, and  $s_r = 1$  to a sphere

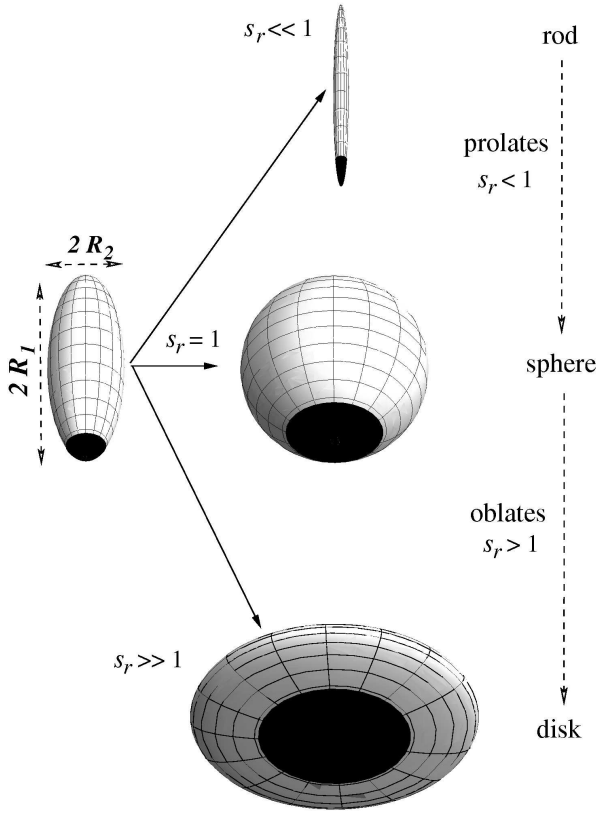


**Fig. 2.** A schematic representation of the spheroidal shapes and of the limiting cases which are discussed in the main text;  $s_r = R_2/R_1$  is varied by varying  $R_2$  while keeping  $R_1$  fixed.

(see Fig. 2). The various spheroidal shapes, i.e., the values of  $s_r$  in the full range  $0 < s_r < \infty$ , are systematically explored by considering the parameter  $R_1$  fixed (introducing a characteristic length scale) while varying the parameter  $R_2$ . The cartesian coordinate system is chosen such that for prolates the foci of the generating (through rotation around its *major* axis) ellipse are located on the  $z$  axis symmetrically with respect to the origin  $O$  which is located at the geometrical center of the particle; correspondingly, for oblates the foci of the generating (through rotation around its *minor* axis) ellipse are located in the  $xy$  plane symmetrically with respect to the origin  $O$ . The ratio  $s_h = h/R_1$  between the height of the cap-like catalyst covered area and the polar semi-axis characterizes the fraction of the particle surface covered by catalyst. Note that the case of a particle with a point-like catalytic site located at one of its poles can be included in the model by considering the limit  $\{s_h \rightarrow 0, \sigma \rightarrow \infty\}$  under the constraint that  $\sigma \times s_h$  is finite (see, c.f., Appendix B). Therefore, by varying the parameters  $s_r$  and  $s_h$  the geometries studied in the literature are recovered as the following limiting cases (see also Ref. [18, (a)]):

- $\{s_r \rightarrow 1^-, 0 < s_h < 1\}$  (where  $1^-$  indicates that the limit is taken through prolate shapes, i.e.,  $s_r \lesssim 1$ ) corresponds to a sphere partially covered by catalyst as in Ref. [11]. (Note that it can be similarly obtained

through oblate shapes, i.e.,  $s_r \gtrsim 1$ , as the limiting case  $\{s_r \rightarrow 1^+, 0 < s_h < 1\}$ );

- $\{s_r \rightarrow 1^-, s_h \rightarrow 0\}$  (or, equivalently,  $\{s_r \rightarrow 1^+, s_h \rightarrow 0\}$ ) with  $\sigma s_h$  finite corresponds to a sphere (obtained as the limit of prolate or oblate shapes, respectively) with a point-like catalytic site as in Ref. [7];
- $\{s_r \ll 1, 0 < s_h < 1\}$  corresponds to the limit of a needle-like particle, which approximates an elongated cylinder (rod) partially covered by catalyst as considered in Refs. [2, 8, 11].

Additionally,

- $\{s_r \gg 1, 0 < s_h < 1\}$  approximates a thin disk partially covered by catalyst.

In general, the chemical conversion of a solvent generates several types of product molecules. Here we shall focus on the particular case in which the chemical conversion  $A \xrightarrow{\text{cat}} A' + B$  of a solvent molecule ( $A$ ) leads to two molecules ( $A'$  and  $B$ ) only, one very similar in size and properties with the solvent itself ( $A' \approx A$ ), the other one ( $B$ ) significantly different. In the following only this latter is denoted as “product molecule” and plays the role of a solute in the solvent. In other words, we consider a situation in which the net result of the chemical conversion can be approximated as the generation of a solute, solely, and in which the reaction does not lead to a solvent depletion near the catalytic site (which otherwise would act as a solvent sink). For example, this is approximately the case for the Pt catalyzed decomposition of hydrogen peroxide ( $\text{H}_2\text{O}_2$ ) in aqueous solution into water ( $\text{H}_2\text{O}$ ) and oxygen ( $\text{O}_2$ ) molecules, as discussed in Refs. [9, 4]. In these experimental studies the oxygen plays the role of the product molecule the properties of which differ significantly from those of the solvent. Here the solvent is actually a binary liquid mixture of  $\text{H}_2\text{O}$  and  $\text{H}_2\text{O}_2$  for which  $\text{H}_2\text{O}$  is chemically passive and does not participate in the chemical conversion.

We thus assume that the reaction at the catalytic zone, i.e., the cap-like area centered around the pole at  $-R_1\hat{e}_z$  (where  $\hat{e}_z$  is the unit vector of the  $z$ -axis), acts effectively only as an ensemble of independent sources – uniformly distributed over the cap area [with number density  $\sigma$  (number of catalytically active sites/unit area)] – of product molecules of diameter  $a$ , which are diffusing into the solvent with diffusion coefficient  $D$  [11]. We shall focus on the case in which the reaction rate  $\nu_B$  at a catalytic site, i.e., the number of product molecules created per unit time, is independent of time. The number density of product molecules is considered to be so low that among themselves they behave like an ideal gas. There is an interaction potential between the product molecules and the moving particle, which includes the impermeability condition at the surface of particle. The interactions between the product molecules and the solvent are accounted for in an effective way via the Stokes - Einstein expression  $D = k_B T / (3\pi\mu a)$  for the diffusion coefficient  $D$  of the product molecules [19], where  $k_B$  is the Boltzmann constant,  $T$  is the temperature, and  $\mu$  is the viscosity of the solution (solvent plus the solute, i.e., the product molecules).

### 3 Phoretic velocity

#### 3.1 General considerations

The presence of a source of solute (product molecules) on parts of the surface of the particle creates a non-uniform and time dependent distribution of solute in the solution (see Fig. 1), i.e., a non-uniform composition of the solution. The solute number density  $\rho(\mathbf{r}, t)$  is characterized by two important features. On the scale of the particle size  $\min(R_1, R_2) \gg a$ ,  $\rho$  varies due to the diffusion process. On the much smaller length scale of the solute diameter  $a$ ,  $\rho(\mathbf{r}, t)$  varies also near the particle surface because it interacts with the particle via an *effective* substrate potential  $\Psi$  (in the sense that  $\Psi$  describes the interaction of the solute molecule with the particle in the presence of the solvent). Typically the range  $\delta$  of  $\Psi$  is proportional to the solute diameter  $a$ . Accordingly the solute molecules interact directly with the particle only if they are within a thin surface film of thickness  $\delta$ , which is assumed to be not deformed by the motion of the particle [12].

In what follows, we assume that the solvent can be considered as a continuum with constant density  $\rho_{solv}$  even at the length scale  $\delta$ , such that a hydrodynamic description applies within the aforementioned surface film. Within this picture the solute molecules and their effective interaction with the particle are replaced by a corresponding distribution of “point forces” acting on the solvent in the film. Within the limitations of such an approach the hydrodynamic description of the solution naturally splits into that of an “inner” region formed by the surface film and that of an “outer” region formed by the exterior space beyond the surface film. Furthermore we assume that for typical velocities  $V$  in phoresis both the Reynolds number  $\text{Re} \simeq \tilde{\rho}_{solv} V \max(R_1, R_2) / \mu$ , where  $\tilde{\rho}_{solv}$  is the *mass density* of the solvent, and the Peclet number  $\text{Pe} \simeq V \max(R_1, R_2) / D$  are small, such that one can approximate the hydrodynamic description with the creeping flow (Stokes) equations and disregard the convection of the solute compared to its diffusive transport. (Here we have assumed that the magnitude of the hydrodynamic flow velocity  $\mathbf{u}$  is similar to that of the phoretic velocity  $V$ , an assumption which will be justified *a posteriori*.) For a particle of size  $\max(R_1, R_2) = 10 \mu\text{m}$  moving through water (density  $\tilde{\rho} = 10^3 \text{ kg/m}^3$ , viscosity  $\mu = 10^{-3} \text{ Pa s}$ ) with a velocity of the order of  $\mu\text{m/s}$ , which is typical for phoresis, one has  $\text{Re} \simeq 10^{-5}$ . For the diffusion at room temperature ( $k_B T_{room} \sim 4 \times 10^{-21} \text{ J}$ ) of  $\text{O}_2$  ( $a \sim 10^{-10} \text{ m}$ ) in an aqueous  $\text{H}_2\text{O}_2$  solution ( $\mu \simeq 10^{-3} \text{ Pa s}$ ), the Stokes-Einstein relation leads to an estimate  $D \simeq 4 \times 10^{-9} \text{ m}^2/\text{s}$  for the diffusion coefficient (in agreement with Ref. [6]), and thus  $\text{Pe} \simeq 10^{-2}$ . Therefore both latter assumptions are justified.

Following Refs. [12, 20, 11], the ensuing asymmetric, non-uniform solute number density  $\rho(\mathbf{r}, t)$  around the particle will give rise, *within the surface film only*, to a pressure gradient along the surface of the particle. This is the case because the surface film is very thin on the scale of the particle size  $\min(R_1, R_2)$  so that the equilibration of the composition profile of the solution within the surface

film can be assumed to be fast along the direction normal to the surface of the particle compared with the diffusional relaxation time of the composition gradient along the surface of the particle, which typically involves a length scale of the order of  $\max(R_1, R_2)$ . In accordance with our earlier assumption that the solute particles can be considered to form an ideal gas, this implies that near the surface of the particle the spatial variations of  $\rho$  (within the surface film and in the direction normal to the surface of the particle) are given by a Boltzmann distribution  $\exp(-\beta\Psi)$ , where  $\beta = 1/(k_B T)$ , corresponding to the local equilibrium configuration in the presence of the effective interaction potential between the particle and the solute molecules, with a prefactor which depends on the position along the surface of the particle [12]. Mechanical equilibrium of the solvent within the surface film along the direction normal to the surface of the particle (no flow along this direction) requires the pressure gradient along the normal to be equal to the body force densities due to the effective particle-solute interactions. Therefore the pressure within the surface film differs from the “outer” pressure field by an “osmotic pressure” term, i.e., a term proportional to the extra solute density  $\Delta\rho$  in excess to that density in the outer region. Since this osmotic pressure varies along the surface of the particle, there is a pressure gradient along the surface of the particle. This lateral pressure gradient is not balanced by any body force and thus generates shear stress within the surface film. Therefore it induces hydrodynamic flow of the solution along the surface of the particle and entails motion of the particle with a steady-state velocity  $\mathbf{V}$  [21, 22]. Because the system has azimuthal symmetry, the motion is along the  $z$ -axis, i.e.,  $\mathbf{V} = V\hat{\mathbf{e}}_z$ .

We note that in a number of instances a different argument has been used in deriving an expression for the velocity of the particle. It invokes a balance between a Stokes-like viscous friction and a “driving force” produced, e.g., by a spatially non-uniform surface tension (owing to the product molecules changing the composition of the solution) [2, 8]. Such an argument (see, e.g., Ref. [2] and the follow-up Ref. [8] which aimed at improving the description through a more rigorous calculation of the density of product particles) is in sharp contradiction with the generally accepted view that in phoresis the motion of the particle plus the surface film (i.e., the region within which the interaction between the particle and the solute molecules is relevant) is force-free, with the velocity being determined precisely by this requirement [12, 11, 13, 14]. This confusion leads to results which differ from the correct ones roughly by a factor which is the square of the ratio between the size of the particle and the range of the particle-solute interactions; i.e., the predicted values of the velocity are too large by orders of magnitude.

#### 3.2 Phoretic slip and phoretic velocity

As discussed above, the pressure gradient along the surface of the particle, induced by its interaction with the non-uniform distribution  $\rho(\mathbf{r}, t)$  of product molecules within a thin surface film, leads to flow of the solution relative

to the particle. Assuming that  $\rho(\mathbf{r}, t)$  is changing slowly in time, this hydrodynamic flow, considered to be locally planar, translates into a (phoretic) slip-velocity,

$$\mathbf{v}_s(\mathbf{r}_p) = -b\nabla^\Sigma \rho(\mathbf{r}_p), \text{ for } \mathbf{r}_p \in \Sigma_\delta, \quad (1)$$

as a boundary condition for the hydrodynamic flow in the outer region [12,11,13]. In this equation  $\Sigma_\delta$  denotes the outer edge of the surface film (which is a surface at a distance  $\delta$  parallel to the surface  $\Sigma$  of the particle),  $\mathbf{r}_p$  denotes a point  $P$  on  $\Sigma_\delta$ ,  $\nabla^\Sigma$  denotes the projection of the gradient operator onto the corresponding local tangential plane of the surface of the particle (actually of  $\Sigma_\delta$ ; but for the outer problem this can be replaced by  $\Sigma$  because the variations of  $\rho$  are over length scales much larger than  $\delta$ ), while

$$b = \frac{k_B T}{\mu} \Lambda \quad (2)$$

is an effective ‘‘mobility’’ coefficient, and  $\lambda = \sqrt{|\Lambda|}$  is a characteristic length scale. The latter is given in terms of the effective interaction potential  $\Psi$  between the particle and the product molecules. Within a local coordinate system in a small domain of the surface film of width  $\delta$ , centered at position  $\mathbf{r}_p$ ,  $\Psi$  determines the product molecule distribution along the direction  $\hat{y}$  normal to the particle surface and yields [12,13]

$$\Lambda \equiv \Lambda(\mathbf{r}_p) = \int_0^\infty d\hat{y} \hat{y} \left( e^{-\beta\Psi(\hat{y}; \mathbf{r}_p)} - 1 \right). \quad (3)$$

We have explicitly indicated in Eq. (3) that the effective interaction potential  $\Psi$  and, consequently, the length scale  $\lambda$  may vary slowly along the surface of the particle over length scales much larger than the thickness  $\delta$  of the surface film. This is the case because one may reasonably expect that the effective interactions between the particle and the product molecules depends on the local chemical composition of the surface. Thus they can be different in the region  $\Sigma_c$  at the pole which is covered by the catalyst from that at the chemically inert part of the particle surface. We note that such non-uniformity of the surface properties has been also explicitly noted in, e.g., Ref. [2], anticipating that the surface tension of the rod-solution interface is different at the Pt and Au ends of the rod. However, its role was ignored in the analysis there, as well as in the follow-up work in Ref. [8], based on the argument that the density of  $\text{O}_2$  is uniform over the Pt end. Nevertheless, such an argument is clearly contradicted by the theoretically calculated  $\text{O}_2$  density along the surface of the rod which shows significant variations over the whole surface of the rod (see Fig. 4 in Ref. [8]). In a first order approximation one can account for these non-uniform properties along the surface by using a position dependent effective mobility  $b(\mathbf{r}_p)$  [Eq. (2) with  $\Lambda \rightarrow \Lambda(\mathbf{r}_p)$ ], which can attain two values, in the expression of the phoretic slip-velocity [Eq. (1)]. This approach has been pursued in Ref. [11]. In the case of a sharp boundary between the catalyst-covered region and the inert one such an approximation is probably justified. However, if the non-uniform

properties vary smoothly and significantly over the surface, then it becomes unclear if this can be accounted for solely by a piece-wise constant effective mobility  $b(\mathbf{r}_p)$ . In such cases, a detailed analysis of the hydrodynamic flow in the surface film forming the inner region is required for understanding the effects of inhomogeneities on the induced phoretic motion. For example, it has been shown that a solid sphere with position-dependent slip boundary condition immersed in a laminar flow experiences a torque induced by this inhomogeneity [23]. Moreover, in the case of electrophoresis it has already been shown that for a particle with non-uniform surface properties the phoretic motion depends strongly on the details of this non-uniformity, which may give rise to counter-intuitive results such as electrophoresis of spherical particles which are electrically neutral and have a zero mean  $\zeta$ -potential (see, e.g., Refs. [24,25]). But there may be cases in which such coatings by certain catalysts do not significantly change the effective interaction between the particle and the product molecules. Accordingly, here we shall focus on the case in which  $\Psi$ , and thus the effective mobility  $b$ , can be assumed to be constant over the surface of the particle. The general case of an effective interaction potential which varies over the surface of the particle will be discussed elsewhere.

As mentioned above, the dynamics at small Pe numbers implies that the convection of the solute is negligible compared to the diffusive transport, i.e., the diffusion of the solute is apparently decoupled from the hydrodynamic flow. However, a coupling between the density profile of the solute, i.e., the solute diffusion, and the flow of the solution is re-established by Eq. (1) which, in the reference frame co-moving with the particle, represents the boundary condition (BC) at the edge of the surface film for hydrodynamic flow in the outer region. Because there are no forces acting on the solution beyond the surface film, based on the assumption of low Re numbers the hydrodynamic flow in the outer region is obtained as the solution of force free and incompressible Stokes equations subject to the following BCs in the laboratory frame: (i) prescribed velocity  $\mathbf{V} + \mathbf{v}_s$  at the edge  $\Sigma_\delta \simeq \Sigma$  of the surface film (i.e., sticking on the surface of the particle plus a slip velocity  $\mathbf{v}_s$  at the edge of the surface film) and (ii) zero velocity (fluid at rest) far away from the particle. After computing the solution in the outer region, which depends parametrically on the velocity  $\mathbf{V}$  of the particle via the above BC (i), the phoretic velocity is determined by the condition that the motion of the system composed of the particle plus the surface film is force free. Here the cumbersome explicit calculation of the hydrodynamic flow is avoided by using Brenner’s generalized reciprocal theorem [18, (b)], which allows one to express the phoretic velocity of the particle as a surface integral of the phoretic slip velocity weighted by the normal component of the position vector

(see Appendix A and, e.g., Ref. [25]):

$$\begin{aligned} \mathbf{V} &= -\frac{1}{3\mathcal{V}_p} \iint_{\Sigma_\delta} (\hat{\mathbf{n}} \cdot \mathbf{r}_p) \mathbf{v}_s d\Sigma_\delta, \\ V &\simeq \frac{b}{3\mathcal{V}_p} \iint_{\Sigma} (\hat{\mathbf{n}} \cdot \mathbf{r}_p) (\hat{\mathbf{e}}_z \cdot \nabla^\Sigma \rho) d\Sigma, \end{aligned} \quad (4)$$

where the second equality follows by using Eq. (1) to replace  $\mathbf{v}_s$ .

In this equation  $\mathcal{V}_p = (4/3)\pi s_r^2 R_1^3$  denotes the volume of the particle,  $\hat{\mathbf{n}}$  is the unit vector of the direction normal to the surface of the particle, and in the integral we replaced  $\Sigma_\delta$  by  $\Sigma$  because the flow in the outer region varies over length scales which are much larger than the difference  $\delta$  between the two. According to Eq. (4), knowledge of the number density  $\rho$  of product molecules at the outer edge  $\Sigma_\delta$  of the surface film completely determines the velocity  $\mathbf{V}$  of the particle.

### 3.3 Steady-state distribution of product molecules (solute)

After switching on the catalytic reaction there is an initial transient phase during which the distribution  $\rho(\mathbf{r}, t)$  of product molecules builds up. Because we are dealing with an unbounded solvent, one may expect that at long times ( $t \rightarrow \infty$ ) the distribution of product molecules reaches a steady-state distribution  $\rho(\mathbf{r})$ . In what follows, we focus on the motion in the long-time regime (in practice, at times  $t$  much longer than the diffusion time  $t_D = [\max(R_1, R_2)]^2/D$ ; for the numerical estimates from Subsec. 3.1,  $t_D \simeq 2.5$  s) in which  $\rho$  and consequently the phoretic slip  $\mathbf{v}_s$  and the phoretic velocity  $\mathbf{V}$  [see Eqs. (1) and (4), respectively] become time independent. Note that here we implicitly assume that the time-scale  $t_R$  of the rotational diffusion of the polar axis of the particle is sufficiently larger than  $t_D$  such that the steady-state distribution  $\rho(\mathbf{r})$  is attained and translational motion of the particle with uniform velocity  $V$  occurs; at times  $t \gg t_R$  the rotational diffusion of the polar axis leads to a quasi-diffusive behavior of the particle displacement (see, e.g., Refs. [4, 26]). These two regimes are clearly observable in the experiments discussed in Ref. [2] (see, in particular, the supporting information therein).

Within the assumptions that the diffusion of product molecules is fast compared with the convection by the solvent flow, i.e., in the limit of small Peclet numbers, and that the product distribution  $\rho(\mathbf{r})$  in the steady state is undisturbed by the flow, i.e., neglecting any so-called polarization effects of the surface film [12], the steady state distribution  $\rho(\mathbf{r})$  of product molecules in the outer region around the moving particle is governed, in the co-moving frame, by the diffusion equation

$$D\nabla^2 \rho(\mathbf{r}) = 0, \mathbf{r} \in \text{outer region}. \quad (5)$$

This equation is to be solved subject to the BCs of (i) zero density far away from the outer edge  $\Sigma_\delta$  of the surface

film and (ii) at each point  $\mathbf{r} \in \Sigma_\delta$  the product molecules current in the outward direction  $\hat{\mathbf{n}}$  normal to the surface is equal to the total reaction rate in an infinitesimal element of  $\Sigma$  centered at  $\mathbf{r} - \delta\hat{\mathbf{n}}$ . The latter BC holds within the assumption that the surface film is very thin [ $\delta \ll \min(R_1, R_2)$ ] such that in the steady state the lateral transport of product molecules in the surface film is negligible compared to the transport into the outer region along the direction normal to  $\Sigma_\delta$ . Since in the calculation of  $\rho(\mathbf{r})$  we shall replace the values of the coordinates corresponding to  $\Sigma_\delta$  by those of  $\Sigma$ , justified by the same argument that  $\rho(\mathbf{r})$  is expected to vary over length scales which are much larger than  $\delta$ , we shall formally apply the second boundary condition directly on the surface  $\Sigma$  of the particle, rather than on  $\Sigma_\delta$ . Hence, the BCs take the following forms:

$$\rho(|\mathbf{r}| \rightarrow \infty) = 0 \quad (6a)$$

$$-D [\hat{\mathbf{n}} \cdot \nabla \rho(\mathbf{r})]_{\mathbf{r} \in \Sigma} = \nu_B \sigma \Upsilon(\mathbf{r}) \quad (6b)$$

$$=: \nu_B \sigma \begin{cases} 1, & \mathbf{r} \in \text{catalytic cap}, \\ 0, & \text{otherwise}. \end{cases}$$

Examples of steady-state distributions  $\rho(\mathbf{r})$  of the solute (in units of  $\rho_0 = \nu_B \sigma R_1/D$ ), obtained from a direct numerical integration of Eqs. (5) and (6), are shown in Fig. 3. One notes that as expected (see Subsec. 3.1) there are significant density variations over the part of the surface covered by the catalyst. These are more pronounced (in addition to the larger amplitude of the distribution) for the “flatter“ shapes, thus intuitively suggesting a larger resulting phoretic velocity for the more flatter shapes. In the following subsections we derive the solute distributions analytically for any spheroidal shape, which allows us to discuss quantitatively the effect of the shape on the phoretic velocity.

#### 3.3.1 Prolate particles

For a prolate shaped ( $s_r < 1$ ) particle with the catalyst distributed over a cap-like region centered at one of its poles (see Fig. 1), Eq. (5) subject to the BCs given by Eq. (6) is most conveniently solved in terms of the prolate spheroidal coordinates  $(\xi, \phi, \eta)$  (see Ref. [27, (a)]):

$$x = \kappa \sqrt{(\xi^2 - 1)(1 - \eta^2)} \cos \phi, \quad (7)$$

$$y = \kappa \sqrt{(\xi^2 - 1)(1 - \eta^2)} \sin \phi, \quad (8)$$

$$z = \kappa \xi \eta. \quad (9)$$

In these equations  $\xi \geq 1$  and  $-1 \leq \eta \leq 1$  parameterize confocal ellipsoids and hyperboloids of revolution, respectively, which have their foci placed on the  $z$  axis a distance  $2\kappa$  apart and symmetrically with respect to the origin  $O$ , while  $0 \leq \phi < 2\pi$  is the azimuthal angle. The  $xz$  planar cuts through the iso-surfaces in terms of prolate spheroidal coordinates are shown in Fig. 1(b). The choice

$$\kappa = \kappa_p = \sqrt{R_1^2 - R_2^2} = R_1 \sqrt{1 - s_r^2}, \quad (10)$$

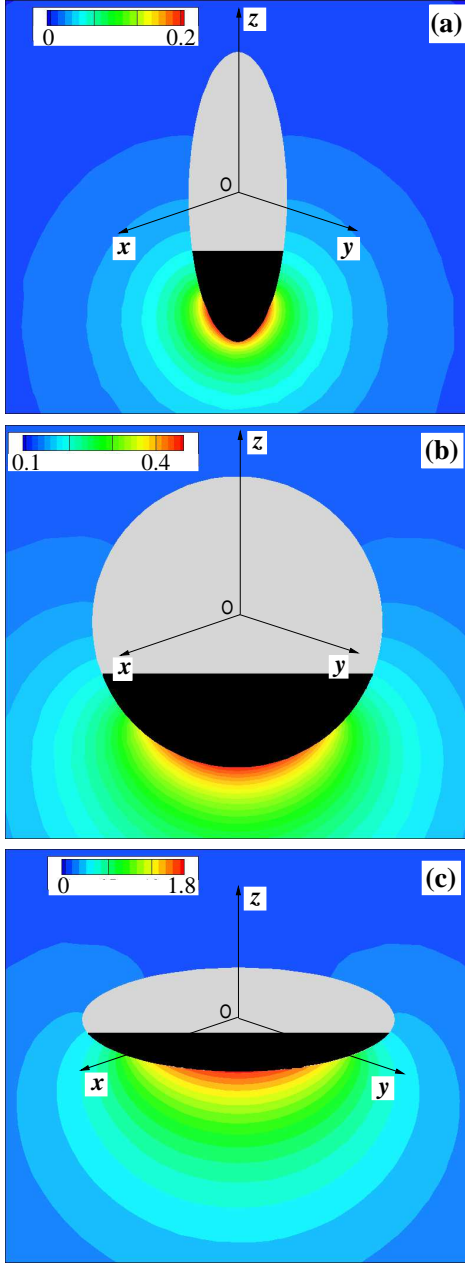


**Fig. 3.** Steady-state distributions  $\rho(\mathbf{r})$  of the solute (in units of  $\rho_0 = \nu_B \sigma R_1/D$ ) around (a) a prolate ( $s_r = 0.3$ ), (b) a spherical ( $s_r = 1$ ), and (c) an oblate ( $s_r = 3.0$ ) particle partially covered by catalyst ( $s_h = 0.3$ ). These distributions are obtained by numerical integration of Eqs. (5) and (6). In each case the color coding of the density ranges from blue (low density) to red (high density) in accordance with the corresponding scale shown on the top left. Note the differences in the scales for (a), (b), and (c).

ensures that the family of ellipsoids includes the one,

$$\xi_0 = \frac{1}{\sqrt{1-s_r^2}} > 1, \quad (11)$$

which corresponds to the surface of the particle [ $\xi_0$  follows from Eqs. (7)-(10) and  $z(\xi_0, \eta = \pm 1; \kappa_p) = R_1$ ]. The outer region thus corresponds to  $\xi > \xi_0$ . Since the intersection of any hyperboloid  $\eta = \text{const}$  from the family defined by  $\kappa_p$  with the surface of the particle is a circle parallel to the equatorial  $xy$  plane, the cap-like region on  $\Sigma$  covered by the catalyst is parameterized by ( $\xi = \xi_0, 0 \leq \phi < 2\pi, -1 \leq \eta \leq \eta_0$ ), where

$$-1 \leq \eta_0 = -1 + s_h \leq 1 \quad (12)$$

[which follows from Eqs. (7)-(11) and  $z(\xi_0, \eta_0; \kappa_p) = -R_1 + h$ , see Fig. 1(a)].

In terms of prolate spheroidal coordinates the solution  $\rho(\xi, \eta)$  of Eq. (5), which has no dependence on  $\phi$  due to the azimuthal symmetry of the system, is finite at  $\eta = \pm 1$  (i.e., on the  $z$  axis), and satisfies the BC in Eq. (6a), can be written as [28, 29]

$$\rho(\xi, \eta) = \sum_{\ell \geq 0} c_\ell Q_\ell(\xi) P_\ell(\eta). \quad (13)$$

$P_\ell$  and  $Q_\ell \equiv Q_\ell^{(0)}$  with [29, 30]

$$\begin{aligned} Q_\ell(w) &:= 2^\ell \sum_{s \geq 0} \frac{(\ell + 2s)! (\ell + s)!}{s! (2\ell + 2s + 1)!} w^{-\ell - 2s - 1} \\ &= \frac{1}{2} P_\ell(w) \ln \frac{w+1}{w-1} - \frac{2\ell-1}{\ell} P_{\ell-1}(w) \\ &\quad - \frac{2\ell-5}{3(\ell-1)} P_{\ell-3}(w) - \dots, \quad w \in \mathbb{C} \setminus [-1, 1], \end{aligned} \quad (14)$$

are the Legendre polynomial and the zeroth-order associated Legendre function of the second kind of degree  $\ell$  (Ref. [27, (b)]), respectively. The terms with  $P_{\ell < 0}$  are, by definition, identically zero. The coefficients  $c_\ell$  are determined by the BC in Eq. (6b). By noting that  $\hat{\mathbf{n}} = \hat{\mathbf{e}}_\xi$ , where  $\hat{\mathbf{e}}_\xi$  is the unit vector corresponding to the  $\xi$  direction, Eq. (6b) can be re-written as

$$-\frac{D}{h_\xi(\xi_0, \eta)} \left( \frac{\partial \rho(\xi, \eta)}{\partial \xi} \right)_{\xi=\xi_0} = \nu_B \sigma \Upsilon(\eta; \eta_0), \quad (15)$$

where  $h_\xi$  is the scale factor corresponding to  $\hat{\mathbf{e}}_\xi$  (with similarly defined scale factors  $h_\eta$  and  $h_\phi$ ) (Ref. [27, (a)]):

$$h_\xi \equiv h_\xi(\xi, \eta) = \kappa_p \sqrt{\frac{\xi^2 - \eta^2}{\xi^2 - 1}}, \quad (16a)$$

$$h_\eta \equiv h_\eta(\xi, \eta) = \kappa_p \sqrt{\frac{\xi^2 - \eta^2}{1 - \eta^2}}, \quad (16b)$$

$$h_\phi \equiv h_\phi(\xi, \eta) = \kappa_p \sqrt{(\xi^2 - 1)(1 - \eta^2)}, \quad (16c)$$

and the parametric dependence of the characteristic function  $\Upsilon(\mathbf{r})$  on  $\eta_0$  [Eq. (6b)] is indicated explicitly. By using the orthogonality of the Legendre polynomials,

$$\int_{-1}^1 d\eta P_n(\eta) P_m(\eta) = \frac{2}{2n+1} \delta_{nm}, \quad (17)$$

where  $\delta_{nm}$  is the Kronecker delta symbol (Ref. [27, (b)]), and by combining Eqs. (13)-(16a), one finds for the coefficients  $c_\ell$ :

$$c_\ell(\xi_0, \eta_0) = -\left(\ell + \frac{1}{2}\right) \frac{\nu_B \sigma R_1}{D} \frac{\gamma_\ell(\xi_0, \eta_0)}{Q'_\ell(\xi_0) \xi_0 \sqrt{\xi_0^2 - 1}} \\ := -\frac{\nu_B \sigma R_1}{D} \tilde{c}_\ell(\xi_0, \eta_0), \quad (18)$$

where  $Q'_\ell(\xi) \equiv dQ_\ell(\xi)/d\xi$  and

$$\gamma_\ell(\xi_0, \eta_0) = \int_{-1}^1 d\eta \sqrt{\xi_0^2 - \eta^2} \Upsilon(\eta; \eta_0) P_\ell(\eta) \\ = \int_{-1}^{\eta_0} d\eta \sqrt{\xi_0^2 - \eta^2} P_\ell(\eta) \quad (19)$$

so that the coefficients  $\tilde{c}_\ell(\xi_0, \eta_0)$  are dimensionless.

### 3.3.2 Oblate particles

For an oblate shaped ( $s_r > 1$ ) particle with the catalyst distributed over a cup-like region centered at one of its poles [see Figs. 1 and 2], Eq. (5) subject to the BCs given by Eq. (6) is most conveniently solved in terms of the oblate spheroidal coordinates  $(\zeta, \phi, \chi)$  (see Ref. [27, (a)]):

$$x = \kappa \sqrt{(\zeta^2 + 1)(1 - \chi^2)} \cos \phi, \quad (20)$$

$$y = \kappa \sqrt{(\zeta^2 + 1)(1 - \chi^2)} \sin \phi, \quad (21)$$

$$z = \kappa \zeta \chi. \quad (22)$$

In these equations  $\zeta \geq 0$  and  $-1 \leq \chi \leq 1$  parameterize confocal ellipsoids and half-hyperboloids of revolution, respectively, which have foci placed symmetrically with respect to the origin O on the  $x$  axis a distance  $2\kappa$  apart, while  $0 \leq \phi < 2\pi$  is the azimuthal angle. Cuts by the  $xz$  plane through the iso-surfaces in terms of oblate spheroidal coordinates are shown in Fig. 1(c). The choice

$$\kappa = \kappa_o = \sqrt{R_2^2 - R_1^2} = R_1 \sqrt{s_r^2 - 1} \quad (23)$$

ensures that the family of ellipsoids includes the one,

$$\zeta_0 = \frac{1}{\sqrt{s_r^2 - 1}} > 0, \quad (24)$$

which corresponds to the surface of the particle;  $\zeta_0$  follows from Eqs. (20)-(23) and  $z(\zeta_0, \chi = \pm 1; \kappa_o) = R_1$ . The outer region thus corresponds to  $\zeta > \zeta_0$ . Since the intersection of any hyperboloid  $\chi = \text{const}$  from the family characterized by  $\kappa_o$  with the surface of the particle is a circle parallel to the equatorial  $xy$  plane, the cap-like region on  $\Sigma$  covered by the catalyst is parameterized by  $(\zeta = \zeta_0, 0 \leq \phi < 2\pi, -1 \leq \chi \leq \chi_0)$ , where

$$\chi_0 = -1 + s_h. \quad (25)$$

This follows from Eqs. (20)-(24) and  $z(\zeta_0, \chi_0; \kappa_o) = -R_1 + h$  [see Fig. 1(a)].

In oblate spheroidal coordinates the solution  $\rho(\zeta, \chi)$  of Eq. (5), which has no dependence on  $\phi$  due to the azimuthal symmetry of the system, is finite at  $\chi = \pm 1$  (i.e., on the  $z$  axis), and satisfies the BC in Eq. (6a), can be written as [29]

$$\rho(\zeta, \chi) = \sum_{\ell \geq 0} m_\ell Q_\ell(i\zeta) P_\ell(\chi), \quad (26)$$

where  $i = \sqrt{-1}$  and [see Eq. (14)]

$$Q_\ell(i\zeta) := 2^\ell \sum_{s \geq 0} \frac{(\ell + 2s)! (\ell + s)!}{s! (2\ell + 2s + 1)!} (i\zeta)^{-\ell - 2s - 1} \\ = -i (\operatorname{arccot} \zeta) P_\ell(i\zeta) - \frac{2\ell - 1}{\ell} P_{\ell-1}(i\zeta) \\ - \frac{2\ell - 5}{3(\ell - 1)} P_{\ell-3}(i\zeta) - \dots \quad (27)$$

The second equation, for which we have used  $(1/2) \ln[(z + 1)/(z - 1)] = \operatorname{arccoth}(z)$  and  $\operatorname{arccoth}(iz) = -i \operatorname{arccot}(z)$ , emphasizes that  $Q_\ell(i\zeta)$  is well defined for all  $\zeta \in \mathbb{R}$  [29]. This is needed because, for  $s_r > \sqrt{2}$ ,  $\zeta_0$  is smaller than 1 [Eq. (24)] and thus the point  $z = i$ , where the Legendre differential equation is singular, lies inside the domain of the solution (in contrast to the case of a prolate, for which  $\xi_0 > 1$ ). The coefficients  $m_\ell$  are determined by the BC in Eq. (6b). Note that because the density  $\rho(\zeta, \chi) \in \mathbb{R}$ , while according to Eq. (27)  $Q_\ell(i\zeta)$  is real (imaginary) for  $\ell$  odd (even), the coefficients  $m_\ell$  in the series representation, Eq. (26) are real (imaginary) for  $\ell$  odd (even).

By using  $\hat{\mathbf{n}} = \hat{\mathbf{e}}_\zeta$ , where  $\hat{\mathbf{e}}_\zeta$  is the unit vector corresponding to the  $\zeta$  direction, Eq. (6b) can be re-written as

$$-\frac{D}{h_\zeta(\zeta_0, \chi)} \left( \frac{\partial \rho(\zeta, \chi)}{\partial \zeta} \right)_{\zeta=\zeta_0} = \nu_B \sigma \Upsilon(\chi; \chi_0), \quad (28)$$

where  $h_\zeta$ ,  $h_\chi$ , and  $h_\phi$  with

$$h_\zeta \equiv h_\zeta(\zeta, \chi) = \kappa_o \sqrt{\frac{\zeta^2 + \chi^2}{1 + \zeta^2}}, \quad (29a)$$

$$h_\chi \equiv h_\chi(\zeta, \chi) = \kappa_o \sqrt{\frac{\zeta^2 + \chi^2}{1 - \chi^2}}, \quad (29b)$$

$$h_\phi \equiv h_\phi(\zeta, \chi) = \kappa_o \sqrt{(\zeta^2 + 1)(1 - \chi^2)}, \quad (29c)$$

are the scale factors corresponding to the  $\hat{\mathbf{e}}_\zeta$ ,  $\hat{\mathbf{e}}_\chi$ , and  $\hat{\mathbf{e}}_\phi$  directions, respectively (Ref. [27, (a)]). By using the orthogonality of the Legendre polynomials [Eq. (17)], and by combining Eqs. (26)-(29a), one finds the following expression for the coefficients  $m_\ell$ :

$$m_\ell(\zeta_0, \chi_0) = -\frac{\nu_B \sigma R_1}{D} \frac{(2\ell + 1) \epsilon_\ell(\zeta_0, \chi_0)}{2 \zeta_0 \sqrt{\zeta_0^2 + 1} [\partial_\zeta Q_\ell(i\zeta)]_{\zeta=\zeta_0}} \\ := -\frac{\nu_B \sigma R_1}{D} \tilde{m}_\ell(\zeta_0, \chi_0), \quad (30)$$



where

$$\begin{aligned}\epsilon_\ell(\zeta_0, \chi_0) &= \int_{-1}^1 d\chi \sqrt{\zeta_0^2 + \chi^2} \Upsilon(\chi; \chi_0) P_\ell(\chi) \\ &= \int_{-1}^{\chi_0} d\chi \sqrt{\zeta_0^2 + \chi^2} P_\ell(\chi)\end{aligned}\quad (31)$$

so that the coefficients  $\tilde{m}_\ell(\zeta_0, \chi_0)$  are dimensionless.

### 3.4 Phoretic velocity of a prolate object.

From differential geometry one has [31]:

(i)  $\nabla^\Sigma = \hat{\mathbf{e}}_\eta \frac{1}{h_\eta} \frac{\partial}{\partial \eta} + \hat{\mathbf{e}}_\phi \frac{1}{h_\phi} \frac{\partial}{\partial \phi}$  and the surface area element is  $d\Sigma = h_\eta h_\phi d\eta d\phi$  because the plane tangent to the surface of the particle is spanned by the unit vectors  $\hat{\mathbf{e}}_\eta$  and  $\hat{\mathbf{e}}_\phi$  of the  $\eta$  and  $\phi$  directions,

(ii)  $\hat{\mathbf{n}} \cdot \mathbf{r} = \hat{\mathbf{e}}_\xi \cdot \mathbf{r} = \frac{x\partial_\xi x + y\partial_\xi y + z\partial_\xi z}{h_\xi} = \frac{\kappa_p^2 \xi}{h_\xi}$ , and

(iii)  $\hat{\mathbf{e}}_z \cdot \nabla^\Sigma \rho(\xi, \eta) = (\hat{\mathbf{e}}_z \cdot \hat{\mathbf{e}}_\eta) \frac{\partial_\eta \rho(\xi, \eta)}{h_\eta} = \frac{\kappa_p \xi}{h_\eta^2} \partial_\eta \rho(\xi, \eta)$ .

By using the expression in Eq. (4) for the phoretic velocity of a *prolate* object one obtains:

$$\begin{aligned}V_{pr} &= \frac{b \xi_0^2}{2R_1} \int_{-1}^1 d\eta \frac{1 - \eta^2}{\xi_0^2 - \eta^2} \partial_\eta \rho(\xi_0, \eta) \\ &= \frac{b \xi_0^2 (\xi_0^2 - 1)^2}{R_1} \int_{-1}^1 d\eta \frac{\eta}{(\xi_0^2 - \eta^2)^2} \rho(\xi_0, \eta) \\ &= -2V_0 \xi_0^2 (\xi_0^2 - 1) \sum_{\ell \geq 0} [\tilde{c}_{2\ell+1}(\xi_0, \eta_0) \\ &\quad \times Q_{2\ell+1}(\xi_0) \int_0^1 d\eta \frac{\eta}{(\xi_0^2 - \eta^2)^2} P_{2\ell+1}(\eta)].\end{aligned}\quad (32)$$

where

$$V_0 = \frac{b\nu_B\sigma}{D}\quad (33)$$

defines the velocity scale.  $V_0$  is expected to be of the order of  $\mu\text{m/s}$ , but because of its dependence on  $b$  it is difficult to provide a theoretical estimate for it. The second equality follows from an integration by parts, while the third one uses the series expansion in Eq. (13) for  $\rho(\xi_0, \eta)$ , Eqs. (10) and (11) to replace  $\kappa_p$  and  $s_r$ , respectively, and the fact that  $P_\ell(\eta)$  is an even (odd) function of  $\eta$  for  $\ell$  even (odd). After replacing  $\tilde{c}_\ell$ ,  $\xi_0$ , and  $\eta_0$  by the corresponding expression in Eqs. (18), (11), and (12), one obtains as final result the phoretic velocity  $V_{pr} \equiv V_{pr}(s_r, s_h; V_0)$  as a function of the geometrical parameters  $s_r$  and  $s_h$ , as well as of the velocity scale  $V_0$ .

### 3.5 Phoretic velocity of an oblate object.

Similar to the calculation in Subsec. 3.4, for an oblate shape one has [31]:

(i)  $\nabla^\Sigma = \hat{\mathbf{e}}_\chi \frac{1}{h_\chi} \frac{\partial}{\partial \chi} + \hat{\mathbf{e}}_\phi \frac{1}{h_\phi} \frac{\partial}{\partial \phi}$  and the surface area element is  $d\Sigma = h_\chi h_\phi d\chi d\phi$ ,

(ii)  $\hat{\mathbf{n}} \cdot \mathbf{r} = \hat{\mathbf{e}}_\zeta \cdot \mathbf{r} = \frac{x\partial_\zeta x + y\partial_\zeta y + z\partial_\zeta z}{h_\zeta} = \frac{\kappa_o^2 \zeta}{h_\zeta}$ , and

(iii)  $\hat{\mathbf{e}}_z \cdot \nabla^\Sigma \rho(\zeta, \chi) = (\hat{\mathbf{e}}_z \cdot \hat{\mathbf{e}}_\chi) \frac{\partial_\chi \rho(\zeta, \chi)}{h_\chi} = \frac{\kappa_o \zeta}{h_\chi^2} \partial_\chi \rho(\zeta, \chi)$ .

By using the expression in Eq. (4) for the phoretic velocity of an *oblate* object one obtains:

$$\begin{aligned}V_{ob} &= \frac{b \zeta_0^2}{2R_1} \int_{-1}^1 d\chi \frac{1 - \chi^2}{\zeta_0^2 + \chi^2} \partial_\chi \rho(\zeta_0, \chi) \\ &= \frac{b \zeta_0^2 (\zeta_0^2 + 1)^2}{R_1} \int_{-1}^1 d\chi \frac{\chi}{(\zeta_0^2 + \chi^2)^2} \rho(\zeta_0, \chi) \\ &= -2V_0 \zeta_0^2 (\zeta_0^2 + 1) \sum_{\ell \geq 0} [\tilde{m}_{2\ell+1}(\zeta_0, \chi_0) \\ &\quad \times Q_{2\ell+1}(i\zeta_0) \int_0^1 d\chi \frac{\chi}{(\zeta_0^2 + \chi^2)^2} P_{2\ell+1}(\chi)].\end{aligned}\quad (34)$$

After replacing  $\tilde{m}_\ell$ ,  $\zeta_0$ , and  $\chi_0$  by the corresponding expressions in Eqs. (30), (24), and (25), one obtains as final result the phoretic velocity  $V_{ob} \equiv V_{ob}(s_r, s_h; V_0)$ . Similar to the case of a prolate object, the terms with even  $\ell$  do not contribute to the phoretic velocity, i.e.,  $m_{\ell \text{ even}} = 0$  because  $P_\ell(\eta)$  is an even (odd) function of  $\chi$  for  $\ell$  even (odd). Note that the expression in Eq. (34) can be obtained from Eq. (32) by the mapping  $\xi \mapsto i\zeta$ ; this is in agreement with similar observations regarding solutions of the Laplace equation in spheroidal coordinates (see, e.g., Ref. [32]), which is a welcome consistency check for our results.

## 4 Discussion

We first note that the length scale  $R_1$  does not enter explicitly into the final expression for the velocity [Eqs. (32) and (34)] which shows that within the assumptions of the model the phoretic velocity of objects with the same aspect ratio but different linear sizes is the same (in agreement with the conclusions of Ref. [11] for spheres and cylindrical rods).

The second observation concerns a symmetry with respect to the area covered by the catalyst. The velocity depends on the ratio  $s_h$ , or equivalently  $\eta_0$  or  $\chi_0$ , via the integral in Eq. (19) and Eq. (31), respectively, which enters into the coefficients of the corresponding series expansion of the density. With  $P_\ell(-\eta) = -P_\ell(\eta)$  for  $\ell$  odd Eq. (19)

yields for  $0 \leq w \leq 1$  and  $\ell$  odd

$$\begin{aligned} \gamma_\ell(\xi_0, \eta_0 = -w) &= \int_{-1}^{-w} d\eta \sqrt{\xi_0^2 - \eta^2} P_\ell(\eta) \\ &= \int_{-1}^w d\eta \sqrt{\xi_0^2 - \eta^2} P_\ell(\eta) \\ &= \gamma_\ell(\xi_0, \eta_0 = w), \end{aligned} \quad (35)$$

because  $\int_{-1}^1 d\eta \sqrt{\xi_0^2 - \eta^2} P_\ell(\eta) = 0$  for  $\ell$  odd. A similar relation holds for the case of an oblate shape:

$$\epsilon_\ell(\zeta_0, \chi_0 = -w) = \epsilon_\ell(\zeta_0, \chi_0 = w). \quad (36)$$

Since  $s_h = 1 + \eta_0 \equiv 1 + \chi_0$ , this means that the coefficients in the series expansion in Eqs. (32) and (34), and thus the velocity of the particle, are the same if the catalytic coverage is less or more than half of the particle by the same amount  $w$ . Equivalently, it means that if the inert and the catalytic characteristics of the two parts of the surface are interchanged, the velocity is the same but the direction of motion is reversed. Therefore, as a function of  $s_h$ ,  $V_{pr}$  and  $V_{ob}$  have an extremum at  $s_h = 1$  ( $\eta_0 = \chi_0 = 0$ ), i.e., if half of the particle surface is covered by the catalyst. For  $s_h = 0$  (no catalyst) or  $s_h = 2$  (entire particle surface covered by the catalyst) and a finite number density  $\sigma$  of catalytic sites, the coefficients  $c_{2\ell+1}$  and  $m_{2\ell+1}$  are identically zero and the velocities predicted by Eqs. (32) and (34) vanish as expected because in these two cases there are no gradients of the density of the product molecules along the surface of the particle.

The dependences on  $\xi_0$  and  $\eta_0$  as well as on  $\zeta_0$  and  $\chi_0$  (i.e., on  $s_r$  and  $s_h$ ) of the series representations of the velocity [Eqs. (32) and (34)] are very complicated and in the general case we have not been able to obtain a solution in closed form. Therefore, we shall study numerically the cases of generic prolate ( $0 < s_r \leq 1$ ) and oblate ( $1 < s_r \leq \infty$ ) shapes, and we shall complement the analysis with analytical results for the limiting cases of a spherical ( $s_r = 1$ ), a needle-like ( $s_r \rightarrow 0$ ), and a disk-like ( $s_r \rightarrow \infty$ ) shaped particle.

For given  $\xi_0$  and  $\eta_0$  ( $\zeta_0$  and  $\chi_0$ ) we approximate the velocity  $V_{pr}$  ( $V_{ob}$ ) by keeping terms up to  $\ell = 15$  in Eq. (32) [Eq. (34)]. This provides a good approximation for all values (a)  $1.001 \leq \xi_0 \leq 80$  (i.e.,  $0.0451 \leq s_r \leq 0.9999$ ) and  $-1 \leq \eta_0 \leq 1$  (prolate shapes) and (b)  $0.01 \leq \zeta_0 \leq 80$  (i.e.,  $1.00008 \leq s_r \leq 100$ ) and  $-1 \leq \chi_0 \leq 1$  (oblate shapes) which we have tested (in the sense that including five additional terms leads to changes in the value of the velocity smaller than  $10^{-6}$ ) [33]. The results for  $V_{pr}/V_0$  and  $V_{ob}/V_0$  are shown in Fig. 4 as functions of  $\eta_0$  and  $\chi_0$  for several values of  $\xi_0$  and  $\zeta_0$ , respectively. The data span the whole range of interest, from  $s_r \ll 1$  (i.e.,  $\xi_0 \gtrsim 1$ ), corresponding to a ‘‘cigar’’ shaped rod, to  $s_r \gg 1$  (i.e.,  $\zeta_0 \ll 1$ ), corresponding to a disk, through  $s_r \simeq 1$  (i.e.,  $\xi_0 \gtrsim 1$  or  $\zeta_0 \gtrsim 1$ ) corresponding to a slightly deformed sphere.

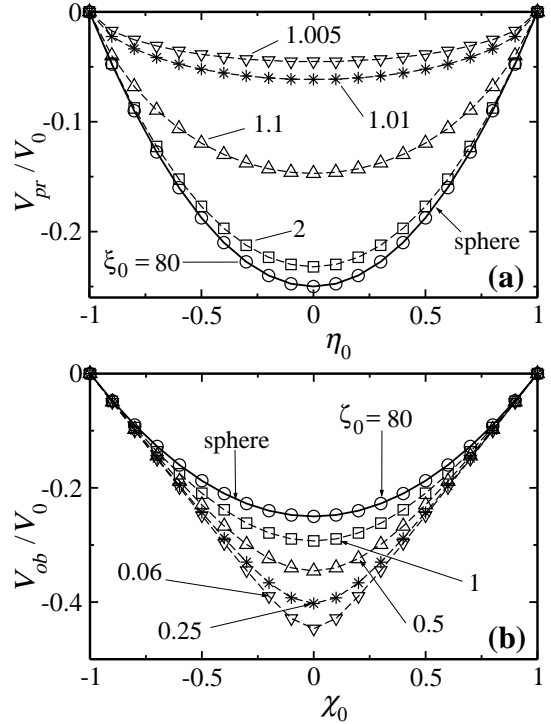


**Fig. 4.** Dependence of the scaled phoretic velocity [Eqs. (32), (34), and (33)] on the fraction  $s_h = 1 + \eta_0 \equiv 1 + \chi_0$  of the surface of the particle covered by the catalyst ( $\eta_0, \chi_0 = -1, 0, 1$  correspond to a particle surface with no catalyst, with the lower half covered by the catalyst, and completely covered by the catalyst, respectively), for (a) a prolate-shaped particle with aspect ratio parameter  $\xi_0 = (1 - s_r^2)^{-1/2} = 80$  ( $s_r = 0.9999$ ), 2 ( $s_r = 0.866$ ), 1.1 ( $s_r = 0.42$ ), 1.01 ( $s_r = 0.14$ ), and 1.005 ( $s_r = 0.099$ ); and (b) an oblate-shaped particle with aspect ratio parameter  $\zeta_0 = (-1 + s_r^2)^{-1/2} = 80$  ( $s_r = 1.00008$ ), 1.0 ( $s_r = 1.41$ ), 0.5 ( $s_r = 2.24$ ), 0.25 ( $s_r = 4.12$ ), and 0.06 ( $s_r = 16.7$ ). The numerical results are shown as symbols; the dashed lines connecting the symbols are guides for the eye. Also shown (solid line) is the exact result [Eq. (65)] corresponding to a spherical particle ( $\xi_0, \zeta_0 \rightarrow \infty$ ).

Figure 4 shows that the dependence of  $V/V_0$  on  $\eta_0$  (or  $\chi_0$ ) is qualitatively the same for all values of  $\xi_0$  and  $\zeta_0$ . The ratio  $V/V_0$  is always negative, which means that  $V$  and  $V_0$  have opposite signs. Therefore, for repulsive effective interactions between the particle and the product molecules, i.e., in the case that  $b < 0$  and thus  $V_0 < 0$ ,  $V$  is positive and the particle moves in the positive  $z$  direction, i.e., ‘‘away’’ from the catalyst covered end. Similarly, for attractive effective interactions the motion will be directed ‘‘towards’’ the catalyst covered end. As expected the velocity curves are symmetric with respect to  $\eta_0 = 0$  and  $\chi_0 = 0$  (i.e.,  $s_h = 1$ ), which is a highly welcome check for the numerical calculations. For a prolate, the minimum at  $\eta_0 = 0$  slowly rises towards zero upon decreasing  $\xi_0$  towards  $\xi_0 = 1^+$ , so that the velocity vanishes for  $s_r = \sqrt{1 - \xi_0^{-2}} \rightarrow 0$ ; as discussed below, this is in qualitative agreement with Refs. [2, 8, 11]. In contrast, for

an oblate the absolute value of the velocity increases upon decreasing  $\zeta_0$  (at fixed  $\chi_0$ ) towards a non-zero and finite limiting value which corresponds to that for an infinitely thin disk (oblate of equatorial diameter much larger than the polar one) [see, c.f., Subsec. 4.3]. (Note that the velocity of such an object remains finite because the product molecules can still “escape” to both sides of the object due to the assumption of an unbounded solvent.) Therefore, we conclude that for a given coverage by catalyst a flatter shape of the particle leads to an increased phoretic velocity. This can be understood intuitively by analyzing the case of a single, point-like catalyst source placed at one of the poles of the particle. The spherically symmetric product number density distribution due to a point-like source but in the absence of the particle will be deformed over a larger extent by an impenetrable boundary which is more elongated transversal to the radial direction than by one more elongated along the radial direction, and thus the gradient along the surface of an oblate particle is expected to be larger than the one corresponding to a prolate particle. Finally, we note that (i) for large values of  $\xi_0$  or  $\zeta_0$  the numerical solutions are in perfect agreement with the known analytical result [Eq. (65)] for a sphere [11]; and that (ii) for very elongated objects (rods or oblates) the results should be considered only as a first-order approximation. This is the case because the analysis leading to the expression in Eq. (1) approximates the flow within the thin surface film as locally planar; such an assumption may break down near the poles for prolates or near the equator for oblates. There for very elongated particles ( $s_r \ll 1$  or  $s_r \gg 1$ ) the curvature of the surface of the particle is very high and cannot be neglected *a priori*.

Further insight can be obtained from an analytical study of the behavior in the limiting cases of a slightly deformed sphere:  $\xi_0 \gg 1$  ( $s_r \lesssim 1$ ) or  $\zeta_0 \gg 1$  ( $s_r \gtrsim 1$ ), of a needle-like shape:  $\xi_0 \gtrsim 1$  ( $s_r \ll 1$ ), and of a disk:  $\zeta_0 \ll 1$  ( $s_r \gg 1$ ) which we shall discuss now.

#### 4.1 Limit of a slightly deformed sphere

We first consider the case in which the limit towards a sphere is taken through prolate shapes, i.e.,  $s_r \rightarrow 1^-$ . Noting that in the limit of a sphere  $s_r = R_2/R_1 \rightarrow 1^-$ , which is equivalent to  $\xi_0 \rightarrow \infty$  [see Eq. (11)], the integral in the last line of Eq. (32) can be approximated as:

$$\begin{aligned} & \int_0^1 d\eta \frac{\eta}{(\xi_0^2 - \eta^2)^2} P_{2\ell+1}(\eta) \\ &= \xi_0^{-4} \left[ \int_0^1 d\eta \eta P_{2\ell+1}(\eta) + \mathcal{O}(\xi_0^{-2}) \right] \\ &= \xi_0^{-4} \left[ \frac{1}{3} \delta_{\ell,0} + \mathcal{O}(\xi_0^{-2}) \right]. \end{aligned}$$

Accordingly, Eq. (32) reduces to

$$\frac{V_{pr}(\xi_0 \gg 1)}{V_0} \simeq - \left[ \xi_0^{-2} (1 - \xi_0^{-2})^{1/2} \frac{\gamma_1(\xi_0) Q_1(\xi_0)}{Q_1'(\xi_0)} \right]_{\xi_0 \gg 1}. \quad (37)$$

Furthermore, Eq. (19) implies

$$\begin{aligned} \gamma_1(\xi_0 \gg 1) &= \xi_0 \left[ \int_{-1}^1 d\eta \Upsilon(\eta; \eta_0) P_1(\eta) \right. \\ &\left. + \frac{1}{2} \xi_0^{-2} \int_{-1}^1 d\eta \eta^2 \Upsilon(\eta; \eta_0) P_1(\eta) + \mathcal{O}(\xi_0^{-4}) \right]; \quad (38) \end{aligned}$$

note that the first integral on the right hand side is equal to twice the velocity (in units of the characteristic velocity  $V_0$ ) corresponding to a spherical particle [Eq. (65), Appendix B]. Due to

$$\left[ \frac{Q_1(\xi_0)}{\xi_0 Q_1'(\xi_0)} \right]_{\xi_0 \gg 1} = -\frac{1}{2} + \frac{3}{10} \xi_0^{-2} + \mathcal{O}(\xi_0^{-4}) \quad (39)$$

and  $V_{sph}/V_0 = (\eta_0^2 - 1)/4$  one finds with  $\eta_0^2 \leq 1$  [Eq. (12)]

$$\begin{aligned} \frac{V_{pr}(\xi_0 \gg 1)}{V_0} &\simeq \left( 1 - \frac{1}{2} \xi_0^{-2} \right) \\ &\times \left[ \frac{V_{sph}}{V_0} + \xi_0^{-2} \int_{-1}^1 d\eta \frac{5\eta^2 - 6}{20} \Upsilon(\eta; \eta_0) P_1(\eta) \right] + \mathcal{O}(\xi_0^{-4}) \\ &= \frac{V_{sph}}{V_0} \left( 1 - \frac{1}{2} \xi_0^{-2} \right) \left( 1 + \frac{5\eta_0^2 - 7}{20} \xi_0^{-2} \right) + \mathcal{O}(\xi_0^{-4}) \\ &\simeq \frac{V_{sph}}{V_0} \left( 1 - \frac{17 - 5\eta_0^2}{20} \xi_0^{-2} \right) \geq \frac{V_{sph}}{V_0}, \quad (40) \end{aligned}$$

where the last inequality follows because the velocity ratios are negative quantities. Equation (40) thus implies that the absolute value of the velocity of a sphere slightly deformed towards a prolate shape ( $\xi_0 \gg 1$ ) is *smaller* than that of a sphere and becomes equal to it in the limit of a vanishing deformation ( $\xi_0 \rightarrow \infty$ ), in agreement with the numerical findings shown in Fig. 4(a).

A similar calculation can be performed for the case in which the limit is taken through oblate shapes, i.e.,  $s_r \rightarrow 1^+$ , which is equivalent to  $\zeta_0 \rightarrow \infty$  [see Eq. (24)], by starting from the integral in the last line of Eq. (34). Following the same steps as above and noting that

$$\left[ \frac{Q_1(i\zeta_0)}{\zeta_0 [\partial_\zeta Q_1(i\zeta)]_{\zeta_0}} \right]_{\zeta_0 \gg 1} = -\frac{1}{2} + \frac{3}{10} \zeta_0^{-2} + \mathcal{O}(\zeta_0^{-4}) \quad (41)$$

we obtain with  $\chi_0^2 \leq 1$  due to  $\chi_0 = \eta_0$  [see Eqs. (12) and (25)]

$$\begin{aligned} \frac{V_{ob}(\zeta_0 \gg 1)}{V_0} &\simeq \left(1 + \frac{1}{2}\zeta_0^{-2}\right) \\ &\times \left[ \frac{V_{sph}}{V_0} - \zeta_0^{-2} \int_{-1}^1 d\chi \frac{5\chi^2 - 6}{20} \mathcal{R}(\chi; \chi_0) P_1(\chi) \right] + \mathcal{O}(\zeta_0^{-4}) \\ &= \frac{V_{sph}}{V_0} \left(1 + \frac{1}{2}\zeta_0^{-2}\right) \left(1 - \frac{5\chi_0^2 - 7}{20} \zeta_0^{-2}\right) + \mathcal{O}(\zeta_0^{-4}) \\ &\simeq \frac{V_{sph}}{V_0} \left(1 + \frac{17 - 5\chi_0^2}{20} \zeta_0^{-2}\right) \leq \frac{V_{sph}}{V_0}, \end{aligned} \quad (42)$$

because the velocity ratios are negative quantities. Thus the absolute value of the velocity of a sphere slightly deformed towards an oblate shape ( $\zeta_0 \gg 1$ ) is *larger* than that of a sphere, while in the limit of a vanishing deformation ( $\zeta_0 \rightarrow \infty$ ) it indeed reduces to the velocity of a spherical particle, again in agreement with the numerical findings shown in Fig. 4(b).

#### 4.2 Limit of a needle-like particle

In this subsection we focus on estimating the asymptotic behavior of the velocity of a half-covered ( $s_h = 1$ ,  $\eta_0 = 0$ ) prolate particle with increasing elongation towards a needle-like shape ( $s_r \ll 1$ , i.e.,  $\xi_0 \gtrsim 1$ ). As shown in Fig. 4(a), for given  $s_r \leq 1$  (or, equivalently,  $\xi_0 > 1$ ) the absolute value of the velocity for any value  $\eta_0 \neq 0$  is smaller than the one for  $\eta_0 = 0$ . Thus the asymptotic behavior of  $|V_{pr}(\xi_0 \rightarrow 1^+, \eta_0)|$  has an upper bound given by  $|V_{pr}(\xi_0 \rightarrow 1^+, \eta_0 = 0)|$ .

Eq. (32) may be re-written as:

$$\begin{aligned} V_{pr}(\xi_0, \eta_0 = 0) &= \frac{b\xi_0^2}{2R_1} \int_{-1}^1 d\eta \left(1 - \frac{\xi_0^2 - 1}{\xi_0^2 - \eta^2}\right) \partial_\eta \rho(\xi_0, \eta) \\ &\stackrel{Eq. (13)}{=} \frac{b\xi_0^2}{2R_1} [\rho(\xi_0, \eta = 1) - \rho(\xi_0, \eta = -1)] \\ &\quad - \frac{b\xi_0^2}{2R_1} (\xi_0^2 - 1) \\ &\quad \times \sum_{\ell \text{ odd}} c_\ell(\xi_0, \eta_0 = 0) Q_\ell(\xi_0) \int_{-1}^1 d\eta \frac{1}{\xi_0^2 - \eta^2} \frac{dP_\ell}{d\eta} \\ &\stackrel{Eq. (13)}{=} \frac{b\xi_0^2}{R_1} \sum_{\ell \text{ odd}} c_\ell(\xi_0, \eta_0 = 0) Q_\ell(\xi_0) \\ &\quad \times \left[ 1 - \frac{\xi_0^2 - 1}{2} \int_{-1}^1 d\eta \frac{1}{\xi_0^2 - \eta^2} \frac{dP_\ell}{d\eta} \right], \end{aligned} \quad (43)$$

where we have used  $P_\ell(1) = 1$  [27, (c)] and the fact that for even indices  $\ell$  the integrals are identically zero because in this case  $P_\ell(\eta)$  is an even function of  $\eta$  so that the integrands are odd functions of  $\eta$ . For odd  $\ell$  the derivative

$dP_\ell/d\eta$  is a polynomial of order  $\ell - 1$  containing only even powers of  $\eta$ . Thus it can be written as

$$\tilde{p}_{\ell-1}(\eta) := \frac{dP_\ell}{d\eta} = \tilde{\beta}_\ell(\xi_0) + (\xi_0^2 - \eta^2) \tilde{q}_{\ell-3}(\eta; \xi_0), \quad (44)$$

where

$$\tilde{\beta}_\ell(\xi_0) = \left( \frac{dP_\ell}{d\eta} \right)_{\eta=\xi_0}. \quad (45)$$

By construction the second term in Eq. (44) must vanish for  $\eta = \xi_0$ . Since  $dP_\ell/d\eta$  depends on  $\eta$  only via  $\eta^2$ , this vanishing must exhibit a prefactor  $\xi_0^2 - \eta^2$  multiplying a polynomial  $\tilde{q}_{\ell-3}(\eta; \xi_0)$  of degree  $(\ell - 3)$  with  $\tilde{q}_{m < 0} \equiv 0$ . Accordingly, the integral in the last equation of Eq. (43) is approximated by

$$\begin{aligned} \int_{-1}^1 d\eta \frac{1}{\xi_0^2 - \eta^2} \frac{dP_\ell}{d\eta} &= -\frac{\tilde{\beta}_\ell(\xi_0)}{\xi_0} \ln \frac{\xi_0 - 1}{\xi_0 + 1} + \int_{-1}^1 d\eta \tilde{q}_{\ell-3}(\eta; \xi_0) \\ &\stackrel{\xi_0 \rightarrow 1^+}{\rightarrow} -\tilde{\beta}_\ell(\xi_0 = 1) \ln(\xi_0 - 1). \end{aligned} \quad (46)$$

This implies that in the limit  $\xi_0 \rightarrow 1^+$  the second term in the square bracket in Eq. (43) vanishes  $\sim (\xi_0 - 1) \ln(\xi_0 - 1)$  and therefore it is a subdominant contribution to the quantity in the square bracket. Thus Eqs. (43) and (46) lead to the following approximation for the velocity of a very elongated prolate towards a needle-like shape ( $\xi_0 \rightarrow 1^+$ ):

$$\begin{aligned} V_{pr}(\xi_0 \gtrsim 1, \eta_0 = 0) &\rightarrow \frac{b\xi_0^2}{R_1} \\ &\times \sum_{\ell \text{ odd}} c_\ell(\xi_0, \eta_0 = 0) Q_\ell(\xi_0) \left[ 1 + \tilde{\beta}_\ell(1) (\xi_0 - 1) \ln(\xi_0 - 1) \right] \\ &\rightarrow \frac{b\xi_0^2}{R_1} \sum_{\ell \text{ odd}} c_\ell(\xi_0, \eta_0 = 0) Q_\ell(\xi_0) \\ &\stackrel{Eq. (18)}{\rightarrow} \frac{V_0}{2\sqrt{2}\sqrt{\xi_0 - 1}} \\ &\times \sum_{\ell \text{ odd}} (2\ell + 1) \left[ \frac{Q_\ell(\xi_0)}{Q'_\ell(\xi_0)} \gamma_\ell(\xi_0, \eta_0 = 0) \right]_{\xi_0 \gtrsim 1}. \end{aligned} \quad (47)$$

Within this approximation the velocity of a very thin, needle-like prolate object is proportional to the difference between the values of the product molecules density at the two ends ( $\eta = \pm 1$ ) of the object. (Note that because of this subtraction only those terms with odd  $\ell$  occur in the series representation of the velocity.) This is similar to the results for a cylindrical thin rod postulated in Ref. [2] and derived in Ref. [11] by invoking a ‘‘slender-body’’ approximation.

Although the above approximation leads to a significantly simplified expression for the velocity, we have been unable to further simplify the resulting series and thus we have studied it numerically. The conclusion of this analysis, the details of which are presented in Appendix C, is

that for  $\xi_0 \gtrsim 1$  the series in Eq. (47) behaves as

$$\begin{aligned} \tilde{f}(\xi_0) &:= \sum_{\ell \text{ odd}} (2\ell + 1) \left[ \frac{Q_\ell(\xi_0)}{Q'_\ell(\xi_0)} \gamma_\ell(\xi_0, \eta_0 = 0) \right]_{\xi_0 \gtrsim 1} \\ &\rightarrow (\xi_0 - 1) \ln(\xi_0 - 1) f(\xi_0), \end{aligned} \quad (48)$$

where

$$f(\xi_0 \gtrsim 1) \simeq -1.5 \times [-\ln(\xi_0 - 1)]^{-0.9}. \quad (49)$$

Equations (47) and (49) therefore render in the limit  $\xi_0 \rightarrow 1^+$

$$\begin{aligned} \frac{V_{pr}(\xi_0 \gtrsim 1, \eta_0 = 0)}{V_0} &\simeq \frac{1.5}{2\sqrt{2}} \sqrt{\xi_0 - 1} \ln(\xi_0 - 1) \\ &\times [-\ln(\xi_0 - 1)]^{-0.9} < 0. \end{aligned} \quad (50)$$

In agreement with the behavior observed for a general prolate shape [see Fig. 4(a)], the velocity (in units of  $V_0$ ) is negative. For  $\xi_0 \rightarrow 1^+$ , the velocity vanishes *faster* than  $\sqrt{\xi_0 - 1} \ln(\xi_0 - 1)$ , i.e., more rapidly than the behavior predicted by Refs. [11,2]. This difference can be either due to an intrinsic difference between the cylinder-like and the needle-like shapes, or, most likely, due to the additional approximations employed in Refs. [11,2] upon computing the solute density distribution (such as using a distribution of point sources in unbounded space and the absence of sources on the flat ends of the cylinder).

We note that in terms of an effective power law the value 0.9 of the exponent in Eq. (49) provides a very good approximation for the behavior of  $f(\xi_0)$  over the physically accessible range of values  $\xi_0 \rightarrow 1^+$ , which can be estimated to be bounded from below by  $\xi_0 \simeq 1 + 10^{-9}$  [i.e., the value corresponding to a 10  $\mu\text{m}$  long carbon nanotube of 1 nm diameter ( $s_r = 10^{-4}$ )]. However, in a strictly mathematical sense, the limiting behavior of  $f(\xi_0 \rightarrow 1^+)$  appears to be not given by Eq. (49) because one finds that the exponent decreases as the range  $\xi_0$  under consideration corresponds to smaller and smaller values; e.g., the exponent reaches the value 0.7 for  $\xi_0 \gtrsim 1 + 10^{-128}$ .

### 4.3 Limit of a disk

In this subsection we focus on the case of a half-covered ( $s_h = 1$ ,  $\chi_0 = 0$ ), very flat oblate (disk-like shape,  $\zeta_0 \ll 1$ ) because among the class of spheroids we have studied this is the one which exhibits the largest absolute value of the velocity.

For  $\zeta_0 \ll 1$ , the coefficients  $\epsilon_n$  with an odd index  $n = 2\ell + 1$  [Eq. (31)] can be approximated by

$$\begin{aligned} \epsilon_{2\ell+1}(\zeta_0 \ll 1, \chi_0 = 0) &\simeq \int_{-1}^{\chi_0=0} d\chi (-\chi) P_{2\ell+1}(\chi) \\ &= -\frac{1}{2} \int_{-1}^1 d\chi P_1(\chi) P_{2\ell+1}(\chi) = -\frac{1}{3} \delta_{\ell,0}. \end{aligned} \quad (51)$$

(According to Subsec. 3.5 the coefficients  $\epsilon_{2\ell}$  do not contribute to  $V_{ob}$ .) Therefore in this limiting case only the first term in the series representation given in Eq. (34) contributes. Since

$$\begin{aligned} \left. \frac{Q_1(i\zeta_0)}{[\partial_\zeta Q_1(i\zeta)]_{\zeta=\zeta_0}} \right|_{\zeta_0 \ll 1} &= \left. \frac{-1 + \zeta_0 \operatorname{arccot}(\zeta_0)}{-\frac{\zeta_0}{1 + \zeta_0^2} + \operatorname{arccot}(\zeta_0)} \right|_{\zeta_0 \ll 1} \\ &\simeq -\frac{2}{\pi} \end{aligned} \quad (52)$$

and

$$\left. \int_0^1 d\chi \frac{\chi}{(\zeta_0^2 + \chi^2)^2} P_1(\chi) \right|_{\zeta_0 \ll 1} \simeq \frac{1}{2} \zeta_0^{-1} \operatorname{arccot}(\zeta_0), \quad (53)$$

one obtains

$$\begin{aligned} V_{ob}(\zeta_0 \ll 1, \chi_0 = 1) &\simeq -\frac{1}{2} \sqrt{1 + \zeta_0^2} V_0 \\ &\rightarrow -\frac{1}{2} V_0 \text{ for } \zeta_0 \rightarrow 0. \end{aligned} \quad (54)$$

Thus in our context the maximal velocity of a spheroidal object is  $|V_0/2|$  and it is realized for a particle with a disk-like shape and such that one side is covered by catalyst and the other one is inert. This is in agreement with the numerical results in Fig. 4.

The general case  $\chi_0 \neq 0$  can be studied in a similar way, but due to the fact that in this case *all* coefficients  $\epsilon_\ell$  with  $\ell$  odd will contribute [see Eq. (31) with  $\chi_0 \neq 0$ ] to the series representation in Eq. (34), the resulting velocity has to be calculated numerically.

## 5 Summary

We have studied the diffusio-phoretic velocity of a spheroidal-shaped particle (Fig. 1) which self-propels by creating gradients of product molecules in a surrounding, unbounded solvent (Fig. 3). Our calculations yield the dependence of the velocity on the shape of the particle, i.e., the aspect ratio between the polar and the equatorial diameters, and on the fraction of the surface of the dissolved particle which is catalytically active in providing product molecules via chemical reactions.

The analysis of our model is based on recasting it in the framework of the standard theory of phoresis. In this context we have critically analyzed the assumptions involved in such an approach, some of them already present in the standard theory, others arising as a result of the mapping of such “active” surface particles into the framework of a theory developed to describe the case of inert particles immersed in a pre-defined, externally controlled concentration gradient. Within the confines of the standard theory of phoresis, we have shown that, irrespective of the shape and of the fraction of the surface covered by the catalyst, the phoretic velocity of the particle depends on its geometry only via the aspect ratio but it is independent of its

absolute size. The numerical analysis of the series representation for the phoretic velocity has been complemented by analytical results for the asymptotic cases of spherical and needle-like particles (Fig. 2). For a given coverage of the particle surface by the catalyst, the absolute value of the velocity of a prolate particle is maximal for an almost spherical particle and decreases gradually towards zero with increasing elongation of the prolate towards a needle-like shape [Fig. 4(a)]. We performed thorough numerical studies (Fig. 5) of the decay of the velocity with increasing elongation ( $R_1 \gg R_2$ , see Fig. 1) and concluded that over the whole physically accessible range  $\xi_0 \gtrsim 1 + 10^{-9}$  it decays effectively  $\sim \left(\frac{R_2}{R_1} \ln \frac{R_2}{R_1}\right) \left(-\ln \frac{R_2}{R_1}\right)^{-0.9} = -\frac{R_2}{R_1} \left(-\ln \frac{R_2}{R_1}\right)^{0.1}$ , which is faster than the previously predicted  $\left(\frac{R_2}{R_1} \ln \frac{R_2}{R_1}\right)$  behavior [11, 2, 8]; this difference is most likely due to the approximations employed in these previous calculations. Our numerical study also indicates that this conclusion of a faster decay than previously predicted holds in the limit (of pure mathematical interest)  $\xi_0 \rightarrow 1^+$  (see the inset in Fig. 5), but we could not determine the exact analytical form of this decay. In contrast, an oblate-shaped particle moves faster with increasing flattening from an almost spherical towards a disk-like shape [Fig. 4(b)]. For a given shape the maximal absolute value of the velocity  $V$  in units of the characteristic velocity  $V_0$  is always attained at half-coverage by the catalyst and varies from 0 (needle) over  $1/4$  (sphere) to  $1/2$  (disk). Therefore, experimental realizations of such self-propelled particles call for a compromise on one hand between the increased speed of flatter particles and their decreased uni-directionality due to, e.g., the unavoidable thermal noise of the solvent and the density fluctuations of the product molecules, and on the other hand between the increased stability against rotations of more elongated particles and their reduced velocity. The results for the phoretic velocity  $V/V_0$  shown in Fig. 4 allow one to directly compare them with experimental realizations, e.g., confocal microscopy studies of micron sized needle-, sphere-, and disk-shaped particles, both qualitatively – the symmetry with respect to the half-covered case and the dependence on the aspect ratio  $s_r = R_2/R_1$  of the shape – as well as quantitatively: the velocity of a half-covered disk is twice that of a spherical particle of the same radius.

As we pointed out in our discussion of the connection between the phoretic slip and the number density gradients of product molecules (Subsec. 3.2), a natural extension of the present study would be to consider in detail the generic case in which the effective interaction potential between the product molecules and the particle differs on the catalyst-covered part of the particle surface from that on the bare one. Other questions of further interest are the influence of curvature on the phoretic velocity in the case of very elongated or very flat spheroidal particles and the influence of external boundaries on both the veloc-

ity and the uni-directionality of the motion for spheroidal particles with axial symmetry.

## Acknowledgements

M.N.P. acknowledges partial financial support by the ‘‘Supported Researcher’’ scheme of the University of South Australia and by the Max-Planck-Institut für Metallforschung (MPI-MF) in Stuttgart, as well as the hospitality of the MPI-MF Stuttgart. M.N.P. and J.R. gratefully acknowledge the financial support from the Australian Research Council via the ARC Linkage Grant Scheme and from AMIRA International.

## A Derivation of the phoretic velocity

The flow field  $\mathbf{u}(\mathbf{r})$  in the outer region is the solution of the incompressible, force free Stokes equations

$$\nabla \cdot \hat{\mathbf{\Pi}} = 0, \quad \nabla \cdot \mathbf{u} = 0, \quad (55)$$

subject to the boundary conditions

$$\mathbf{u}|_{\Sigma_\delta} = \mathbf{V} + \mathbf{v}_s, \quad \mathbf{u}|_{|\mathbf{r}| \rightarrow \infty} = 0. \quad (56)$$

$\hat{\mathbf{\Pi}} := -p\hat{\mathbf{I}} + \mu\hat{\mathbf{S}}$  is the corresponding pressure tensor, where  $p$  is the hydrostatic pressure and  $\hat{\mathbf{S}}$  is the shear stress tensor, i.e.,  $S_{\alpha\beta} = \partial u_\alpha / \partial x_\beta + \partial u_\beta / \partial x_\alpha$ . Owing to the linearity of the Stokes equations, we can write the solution as  $\mathbf{u} = \mathbf{u}' + \mathbf{u}''$  and  $\hat{\mathbf{\Pi}} = \hat{\mathbf{\Pi}}' + \hat{\mathbf{\Pi}}''$ , where  $\mathbf{u}'$  and  $\mathbf{u}''$  are the solutions of the incompressible Stokes equations which vanish at infinity and satisfy the boundary conditions

$$\mathbf{u}'|_{\Sigma_\delta} = \mathbf{v}_s \quad \text{and} \quad \mathbf{u}''|_{\Sigma_\delta} = \mathbf{V}, \quad (57)$$

respectively, while  $\hat{\mathbf{\Pi}}'$  and  $\hat{\mathbf{\Pi}}''$  are the corresponding pressure tensors. By using the condition that the motion of the particle and the outer hydrodynamic flow are such that there is no net force acting on the system composed of the particle plus the surface film, and by replacing  $\hat{\mathbf{\Pi}}''$  with the expression for the pressure tensor on the surface of an ellipsoid translating through an unbounded fluid at rest [34],

$$\left(\hat{\mathbf{n}} \hat{\mathbf{\Pi}}''\right)_{\Sigma_\delta} = -\frac{1}{3} \frac{\mu}{\mathcal{V}_p} (\hat{\mathbf{n}} \cdot \mathbf{r})_{\Sigma_\delta} \hat{\mathbf{K}}^{(t)} \mathbf{V}, \quad (58)$$

one obtains

$$\iint_{\Sigma_\delta} d\Sigma \hat{\mathbf{n}} \hat{\mathbf{\Pi}}' = - \iint_{\Sigma_\delta} d\Sigma \hat{\mathbf{n}} \hat{\mathbf{\Pi}}'' = \mu \hat{\mathbf{K}}^{(t)} \mathbf{V}. \quad (59)$$

$\hat{\mathbf{n}}$  is the unit vector of the direction normal to  $\Sigma_\delta$  (oriented towards the fluid) and  $\hat{\mathbf{K}}^{(t)}$  is a constant diagonal tensor which depends on the diameters of the particle only; its explicit expression is not needed in the following.

On the other hand, because the pairs  $(\mathbf{u}', \hat{\mathbf{\Pi}}')$  and  $(\mathbf{u}'', \hat{\mathbf{\Pi}}'')$  are, by construction, solutions of the force-free,

incompressible Stokes equations and decay at infinity, they satisfy Brenner's (or Lorentz's) reciprocal theorem [18, (b)]:

$$\iint_{\Sigma_\delta} d\Sigma \hat{\mathbf{n}} \hat{\mathbf{\Pi}}' \mathbf{u}'' = \iint_{\Sigma_\delta} d\Sigma \hat{\mathbf{n}} \hat{\mathbf{\Pi}}'' \mathbf{u}'. \quad (60)$$

By using Eq. (58) to replace  $\hat{\mathbf{\Pi}}''$  and the BCs in Eq. (57) to replace  $\mathbf{u}'$  and  $\mathbf{u}''$ , and by noting that  $\mathbf{V}$  and  $\hat{\mathbf{K}}^{(t)}$  are constant with respect to the integrations, one obtains

$$\mathbf{V} \iint_{\Sigma_\delta} d\Sigma \hat{\mathbf{n}} \hat{\mathbf{\Pi}}' = -\frac{1}{3} \frac{\mu}{\mathcal{V}_p} \hat{\mathbf{K}}^{(t)} \mathbf{V} \iint_{\Sigma_\delta} d\Sigma (\hat{\mathbf{n}} \cdot \mathbf{r}) \mathbf{v}_s. \quad (61)$$

By using Eq. (59) for the rhs of Eq. (61) and then replacing in the calculations  $\Sigma_\delta$  by  $\Sigma$ , one obtains Eq. (4) for the phoretic velocity.

## B Phoretic velocity of a spherical Janus particle

The case of a spherical particle ( $s_r = 1$ ) with a catalytic cap centered at a point chosen as one of its poles (see Fig. 1) has been discussed in Ref. [11]. Thus we provide here only a brief summary of the results for reasons of completeness, further referencing, and provision of some remarks. Equation (5) subject to the BCs given in Eq. (6) can be conveniently solved using the standard polar spherical coordinates  $(r, \theta, \phi)$ . The solution  $\rho(r, \theta)$  of Eq. (5) (there is no dependence on  $\phi$  because the system has azimuthal symmetry) which satisfies the BC in Eq. (6a) is

$$\rho(r, \theta) = \sum_{\ell \geq 0} \frac{d_\ell}{r^{\ell+1}} P_\ell(\cos \theta), \quad (62)$$

where the coefficients  $d_\ell$  are determined by the BC in Eq. (6b). Since the cap-like region on  $\Sigma$  covered by the catalyst can be parameterized by  $(r = R_1, \theta_0 \leq \theta \leq \pi, 0 \leq \phi < 2\pi)$ , where

$$\cos \theta_0 = -1 + s_h, \quad (63)$$

one obtains

$$\begin{aligned} d_\ell &= \frac{2\ell + 1}{2(\ell + 1)} \frac{R_1^{\ell+2}}{D} \int_0^\pi d\theta (\sin \theta) \nu_B \sigma \Upsilon(\theta, \theta_0) P_\ell(\cos \theta) \\ &= \frac{\nu_B \sigma R_1^{\ell+2}}{D} \frac{2\ell + 1}{2(\ell + 1)} \int_{-1}^{+1} dx \Upsilon(x, \cos \theta_0) P_\ell(x) \\ &=: \frac{\nu_B \sigma R_1^{\ell+2}}{D} \tilde{d}_\ell(s_h). \end{aligned} \quad (64)$$

With  $\hat{\mathbf{n}} \cdot \mathbf{r} = r$  and  $\hat{\mathbf{e}}_z \cdot \nabla^\Sigma \rho(R_1, \theta) = -(\sin \theta / R_1) \partial_\theta \rho(R_1, \theta)$ , and by using the expressions in Eqs. (4) and (6b) for the phoretic velocity and for the characteristic function  $\Upsilon(\mathbf{r})$ ,

respectively, one finds:

$$\begin{aligned} V_{sph} &= \frac{b}{R_1} \int_0^\pi d\theta \sin \theta \cos \theta \rho(R_1, \theta) \\ &= \frac{2}{3} V_0 \tilde{d}_1(s_h) = \frac{(1 - s_h)^2 - 1}{4} V_0. \end{aligned} \quad (65)$$

In Eq. (65) the first equality has been derived in Refs. [7, 11]. The second equality follows by using the series expansion in Eq. (62) for  $\rho(R_1, \theta)$  and due to  $\cos \theta = P_1(\cos \theta)$  so that in the expansion all terms with  $\ell \neq 1$  vanish. We note that, as for the general prolate or oblate spheroid, there is no explicit dependence on  $R_1$  [11]. Equation (65) provides the following conclusions:

- (i) Since  $0 \leq s_h \leq 2$ ,  $V_{sph}$  and  $V_0$  have opposite signs. Thus for repulsive interactions between the particle and the product molecules the motion will be in the positive  $z$ -direction because  $b$  and thus  $V_0$  are negative [12, 7]; similarly, for attractive interactions, the motion will be in the negative  $z$ -direction (see Fig. 1).
- (ii) As expected on basis of symmetry considerations, the maximum velocity  $V_{sph}^{\max} = -V_0/4$  occurs for  $s_h = 1$ , i.e., if the catalyst covers just a hemisphere.
- (iii) For any finite value  $\sigma$  of the density of catalytic sites the phoretic velocity vanishes if the surface area covered by the catalyst tends to zero, i.e.,  $V_{sph}(s_h \rightarrow 0; \sigma < \infty) \rightarrow 0$ , as expected intuitively.
- (iv) Since  $2\pi R_1^2 s_h \sigma$  is the total number of catalytic sites in the area covered by the catalyst, the case of a sphere with a single catalytic source corresponds to the limit  $\{s_h \rightarrow 0, \sigma \rightarrow \infty\}$  such that  $2\pi R_1^2 s_h \sigma = 1$ . The phoretic velocity in this case is

$$V_{sph}(\{s_h \rightarrow 0, \sigma \rightarrow \infty, 2\pi R_1^2 s_h \sigma = 1\}) = -\frac{b\nu_B}{4\pi R_1^2 D},$$

in agreement with Ref. [7].

- (v) If a general axially symmetric distribution of catalytic activities  $\nu_B \mapsto \nu_B f(\theta)$  is considered, as in Ref. [11], the second equality in Eq. (65) still holds with the coefficients  $\tilde{d}_\ell$  redefined by the particular choice of the distribution considered by replacing  $\Upsilon(\theta) \mapsto f(\theta) \Upsilon(\theta)$  in the first equation in Eq. (64).

## C Numerical analysis of the velocity in the limiting case of a needle-like particle

According to Eq. (47), the behavior of the velocity of a prolate object in the limit  $\xi_0 \rightarrow 1^+$  is determined by the series

$$\tilde{f}(\xi_0) := \sum_{\ell \text{ odd}} (2\ell + 1) \left[ \frac{Q_\ell(\xi_0)}{Q'_\ell(\xi_0)} \gamma_\ell(\xi_0, \eta_0 = 0) \right]_{\xi_0 \gtrsim 1}. \quad (66)$$

Because  $Q_\ell(\xi_0 \rightarrow 1^+) \sim \ln(\xi_0 - 1)$  [see Eq. (14)], one may expect that for  $\xi_0 \gtrsim 1$  the series above varies as

$$\begin{aligned} \tilde{f}(\xi_0 \rightarrow 1^+) &\simeq (\xi_0 - 1) \ln(\xi_0 - 1) \\ &\times \sum_{\ell \text{ odd}} (2\ell + 1) \gamma_\ell(\xi_0 = 1, \eta_0 = 0) \\ &=: (\xi_0 - 1) \ln(\xi_0 - 1) f(\xi_0 = 1), \end{aligned} \quad (67)$$

where the series defining the prefactor  $f(1) \equiv f(\xi_0 = 1)$  has to be calculated numerically. However, within the limits of numerical accuracy it turns out that  $f(1) = 0$  so that Eq. (67) does not capture the leading behavior of  $\tilde{f}(\xi_0 \rightarrow 1^+)$ . Most likely, the reason for the failure of this approximation is that the series representation of the product density [Eq. (13)] is not uniformly convergent (and actually completely breaks down) at  $\xi_0 = 1$ , where the differential equation of the Legendre functions is singular and  $Q_\ell(\xi_0)$  diverges; consequently, there is no warranty that the limit  $\xi_0 \rightarrow 1^+$  can be taken term by term. The result  $f(1) = 0$  thus suggests that instead the series has to be first summed up for general  $\xi_0$  and only then the sum can be evaluated in the limit  $\xi_0 \rightarrow 1^+$ . (See also Ref. [2], in which the thin rod limit of a vanishing ratio between the radius and the length of a cylinder [i.e., Eq. (4) therein] could be taken only after calculating the velocity as a function of this ratio [Eq. (3) therein]; similar arguments apply to the derivation of Eq. (16) from (14) in Ref. [11].)

We therefore proceed with a numerical study of the series  $\tilde{f}(\xi_0)$  [Eq. (66)] as a function of  $\xi_0 \gtrsim 1$ . By using the recursion relation satisfied by the Legendre  $Q_\ell$  functions [30]

$$Q'_\ell(w) = \frac{\ell + 1}{w^2 - 1} [Q_{\ell+1}(w) - w Q_\ell(w)] \quad (68)$$

and the series representation [Eq. (14)] for  $Q_\ell(w)$ , one concludes that for  $\xi_0 > 1$  and  $\ell \gg 1$  the behavior of the ratio involving the Legendre functions  $Q_\ell$  is given by

$$\left[ \frac{Q_\ell(\xi_0)}{Q'_\ell(\xi_0)} \right]_{\ell \gg 1} \sim \frac{2\xi_0(\xi_0^2 - 1)}{(1 - 2\xi_0^2)} \frac{1}{\ell + 1} < 0. \quad (69)$$

Turning now to the behavior of  $I_\ell(\xi_0) := \gamma_\ell(\xi_0, \eta_0 = 0)$  for  $\xi_0 \gtrsim 1$ , we first note that [Eq. (19)]

$$\begin{aligned} |I_\ell(\xi_0)| &\leq \int_{-1}^0 d\eta \left| \sqrt{\xi_0^2 - \eta^2} P_\ell(\eta) \right| \\ &\leq \xi_0 \int_{-1}^0 d\eta |P_\ell(\eta)| \leq \xi_0. \end{aligned} \quad (70)$$

For large  $\ell$ , i.e.,  $\ell > 50$  and values of  $\xi_0$  very close to 1, i.e.,  $\xi_0 - 1 \lesssim 10^{-6}$ , an accurate direct numerical determination of  $I_\ell(\xi_0)$  [Eq. (19)] is extremely difficult mainly because of the oscillatory behavior of the Legendre polynomials, and one thus has to find a way to reformulate the integral. To this end we make use of the representation of the

Legendre polynomials with *odd* index  $\ell$  in terms of the hypergeometric function  ${}_2F_1$  [30]:

$$\begin{aligned} P_\ell(\eta) &= (-1)^{\frac{\ell-1}{2}} \frac{\ell!}{2^{\ell-1} \left(\frac{\ell-1}{2}!\right)^2} \\ &\times \eta {}_2F_1 \left( -\frac{\ell-1}{2}, \frac{\ell}{2} + 1; \frac{3}{2}; \eta^2 \right) := \alpha_\ell p_\ell(\eta), \end{aligned} \quad (71)$$

where  $\alpha_\ell$  denotes the prefactor and

$p_\ell(\eta) = \eta {}_2F_1 \left( -\frac{\ell-1}{2}, \frac{\ell}{2} + 1; \frac{3}{2}; \eta^2 \right)$  is a polynomial of order  $\ell$ . The hypergeometric function  ${}_2F_1(w)$  obeys the relation [27, (d)]

$$\begin{aligned} \frac{d}{dw} {}_2F_1(a, b; c; w^2) &= 2 \frac{ab}{c} w \\ &\times {}_2F_1(a+1, b+1; c+1; w^2), \end{aligned} \quad (72)$$

with  ${}_2F_1(0, b; c \neq 0; w^2) \equiv 1$  and  ${}_2F_1(a, b; c; 0) = 1$ , and it is well defined, as well as its derivatives, at  $w = 1$  (being polynomials). Accordingly, for  $\ell$  odd,  $I_\ell(\xi_0)$  can be computed via successive integrations by parts:

$$\begin{aligned} I_\ell(\xi_0)/\alpha_\ell &= \int_{-1}^0 d\eta \left[ -\frac{1}{3}(\xi_0^2 - \eta^2)^{3/2} \right]' \\ &\times {}_2F_1 \left( -\frac{\ell-1}{2}, \frac{\ell}{2} + 1; \frac{3}{2}; \eta^2 \right) \\ &= -\frac{1}{3} \xi_0^3 + a_1(\ell, 0)(\xi_0^2 - 1)^{3/2} \\ &+ \left( \frac{2}{3} \right)^2 \left( \frac{1}{2} - \frac{\ell}{2} \right) \left( 1 + \frac{\ell}{2} \right) \\ &\times \int_{-1}^0 d\eta \left[ -\frac{1}{5}(\xi_0^2 - \eta^2)^{5/2} \right]' \\ &\times {}_2F_1 \left( -\frac{\ell-1}{2} + 1, \frac{\ell}{2} + 1 + 1; \frac{3}{2} + 1; \eta^2 \right) \\ &= -\frac{1}{3} \xi_0^3 - \left( \frac{2}{3} \right)^2 \frac{1}{5} \left( \frac{1}{2} - \frac{\ell}{2} \right) \left( 1 + \frac{\ell}{2} \right) \xi_0^5 \\ &+ a_1(\ell, 0)(\xi_0^2 - 1)^{3/2} + a_1(\ell, 1)(\xi_0^2 - 1)^{5/2} \\ &+ \left( \frac{2}{3} \right)^2 \left( \frac{2}{5} \right)^2 \left( \frac{1}{2} - \frac{\ell}{2} \right) \left( \frac{3}{2} - \frac{\ell}{2} \right) \\ &\times \left( 1 + \frac{\ell}{2} \right) \left( 2 + \frac{\ell}{2} \right) \\ &\times \int_{-1}^0 d\eta \left[ -\frac{1}{7}(\xi_0^2 - \eta^2)^{7/2} \right]' \\ &\times {}_2F_1 \left( -\frac{\ell-1}{2} + 2, \frac{\ell}{2} + 1 + 2; \frac{3}{2} + 2; \eta^2 \right) \\ &= \dots \text{ in total } (\ell - 1)/2 \text{ steps,} \\ &\quad \text{until reaching } {}_2F_1(0, b; c; \eta^2) \equiv 1. \end{aligned} \quad (73)$$



The coefficients  $a_1(\ell, k)$  of the terms  $(\xi_0^2 - \eta^2)^{3/2+k}$  are proportional to  ${}_2F_1\left(-\frac{\ell-1}{2} + k, \frac{\ell}{2} + 1 + k; \frac{3}{2} + k; 1\right)$  and can be determined analytically. The terms formed by powers of  $\xi_0$  can be summed up in closed form, and it turns out that they provide a very good approximation for the value of  $I_\ell(\xi_0)$ :

$$\begin{aligned} I_\ell(\xi_0 \gtrsim 1) &\simeq \alpha_\ell \left\{ -\frac{1}{3}\xi_0^3 - \sum_{s=0}^{(\ell-3)/2} \left[ \prod_{m=0}^s \left( \frac{2}{2m+3} \right)^2 \right] \right. \\ &\times \left. \left[ \prod_{m=0}^s \left( \frac{1}{2} - \frac{\ell}{2} + m \right) \left( 1 + \frac{\ell}{2} + m \right) \right] \frac{\xi_0^{2s+5}}{2s+5} \right\} \\ &\simeq \alpha_\ell \left[ -\frac{1}{3}\xi_0^3 + \frac{\ell^2 + \ell - 2}{45} \xi_0^5 \right. \\ &\times \left. {}_3F_2 \left( \left\{ 1, \frac{3}{2} - \frac{\ell}{2}, 2 + \frac{\ell}{2} \right\}; \left\{ \frac{5}{2}, \frac{7}{2} \right\}; \xi_0^2 \right) \right]. \quad (74) \end{aligned}$$

Since Eq. (74), which leads to a polynomial of order  $2\frac{\ell-3}{2} + 5 = \ell + 2$  [see the first equality in Eq. (74)], predicts that at large  $\ell$  and  $\xi_0 > 1$  the behavior is dominated by the term  $\xi_0^{\ell+2}$ , it obviously represents an approximation which breaks down for very large  $\ell$  or for not small enough values of  $\xi_0 - 1$ . However, this breakdown of the approximation in Eq. (74) can be easily monitored by checking that the result obeys the bound given by Eq. (70). The approximation can be systematically improved, if needed, by including the terms  $a_1(\ell, k)(\xi_0^2 - \eta^2)^{3/2+k}$  (which can be computed analytically) as they become relevant. For  $\xi_0 - 1 \leq 10^{-4}$  and  $\ell \leq 201$  ( $\ell$  odd), we did not have to add any such corrections to Eq. (74).

The closed form of Eq. (74) significantly simplifies the numerical study of the behavior of  $I_\ell(\xi_0 \gtrsim 1)$  (with  $\ell$  odd). It strongly supports (by extrapolating the results within the range where it provides an accurate approximation) that  $I_{\ell \rightarrow \infty}(\xi_0) \rightarrow 0$  and that  $\text{sign}[I_\ell(\xi_0)] = \text{sign}(\alpha_\ell) = (-1)^{\frac{\ell-1}{2}}$ . In combination with Eq. (69), this shows that approximating  $I_\ell(\xi_0 \gtrsim 1)$  by Eq. (74) in the series representation of Eq. (66) leads to a general form of the term in the series for  $\tilde{f}(\xi_0)$  which has alternating sign and vanishes with increasing  $\ell$ , which ensures that as expected the series is convergent.

We define the partial sum  $\tilde{f}_L(\xi_0)$ , with  $L$  odd, of the series in Eq. (66) as

$$\begin{aligned} \tilde{f}_L(\xi_0) &= \frac{1}{2} \left( \sum_{\ell=1, \ell \text{ odd}}^L (2\ell+1) \frac{Q_\ell(\xi_0)}{Q'_\ell(\xi_0)} I_\ell(\xi_0) \right. \\ &\quad \left. + \sum_{\ell=1, \ell \text{ odd}}^{L+2} (2\ell+1) \frac{Q_\ell(\xi_0)}{Q'_\ell(\xi_0)} I_\ell(\xi_0) \right), \quad (75) \end{aligned}$$

such that the oscillatory behavior induced by the alternating signs of successive terms is damped. Guided by the logarithmic divergence of  $Q_\ell(\xi_0 \rightarrow 1^+)$ , by the fact that the series defining the prefactor  $f(1)$  [Eqs. (66) and (67)]

turned out to be convergent (although vanishing), and by the results for the phoretic velocity of a rod-like particle in Refs. [11,2], we make the *ansatz* that  $\tilde{f}(\xi_0)$  behaves as

$$\tilde{f}(\xi_0 \gtrsim 1) = \underbrace{(\xi_0 - 1) \ln(\xi_0 - 1)}_{:= r(\xi_0)} f(\xi_0) \quad (76)$$

and aim at determining numerically the function  $f(\xi_0)$ .

In Fig. 5 we show the dependence of  $f_L(\xi_0) = \tilde{f}_L(\xi_0)/r(\xi_0)$  on  $L$  for various values  $\epsilon := \xi_0 - 1$ ,  $10^{-64} \leq \epsilon \leq 10^{-4}$ . The convergence of the partial sums is clear, and this allows us to extract the values  $f(\xi_0)$  as the corresponding constant plateau values of each of the curves  $f_L(\xi_0)$ . The numerically determined  $f(\xi_0)$ , for clarity shown in the inset of Fig. 5 as a function of  $-\log_{10}(\epsilon)$ , highlights the following important features: (i)  $f(\xi_0) < 0$  for all  $\xi_0 \gtrsim 1$ , and (ii) the data set  $\{-\log_{10}(\epsilon), f(\xi_0 = 1 + \epsilon)\}$  is very well fitted by a power law [dashed line in the inset in Fig. 5] leading to  $f(\xi_0 \rightarrow 1^+) \simeq -0.7 [-\log_{10}(\xi_0 - 1)]^{-0.9} \simeq -1.5 [-\ln(\xi_0 - 1)]^{-0.9}$ .

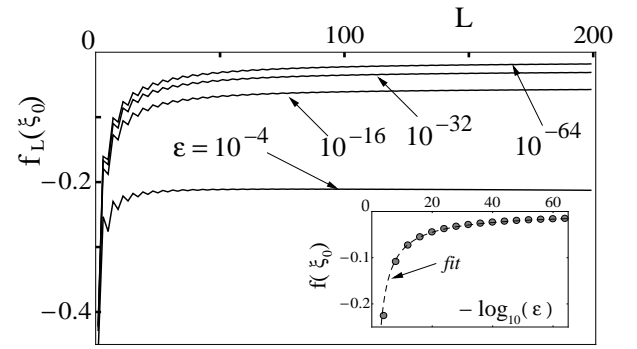


**Fig. 5.** Dependence of  $f_L(\xi_0)$  (see the main text) on  $L$  (for  $L$  odd) for  $\epsilon := \xi_0 - 1 = 10^{-4}, 10^{-16}, 10^{-32}$ , and  $10^{-64}$ . The inset shows the resulting  $f(\xi_0)$  (points) obtained from the extrapolated  $f_{L \rightarrow \infty}(\xi_0)$ , as well as the power law fit  $-0.7 \times [-\log_{10}(\epsilon)]^{-0.9}$  (dashed line), as a function of  $-\log_{10}(\epsilon)$ .

## References

1. R.F. Ismagilov, A. Schwartz, N. Bowden, and G.M. Whitesides, *Angew. Chem., Int. Ed.* **41**, 652 (2002).
2. W.E. Paxton, K.C. Kistler, C.C. Olmeda, A. Sen, S.K.St. Angelo, Y. Cao, T.E. Mallouk, P.E. Lammert, and V.H. Crespi, *J. Am. Chem. Soc.* **126**, 13424 (2004).
3. J.M. Catchmark, S. Subramanian, and A. Sen, *Small* **1**, 1 (2005).
4. J.R. Howse, R.A.L. Jones, A.J. Ryan, T. Gough, R. Vafabakhsh, and R. Golestanian, *Phys. Rev. Lett.* **99**, 048102 (2007).
5. A. Erbe, M. Zientara, L. Baraban, C. Kreidler, P. Leiderer, *J. Phys.: Condens. Matter* **20**, 404215 (2008); L. Baraban, C. Kreidler, D. Makarov, P. Leiderer, A. Erbe, arXiv:0807.1619v1.
6. W.E. Paxton, S. Sundararajan, T.E. Mallouk, and A. Sen, *Angew. Chem., Int. Ed.* **45**, 5420 (2006).

7. R. Golestanian, T.B. Liverpool, and A. Ajdari, *Phys. Rev. Lett.* **94**, 220801 (2005).
8. N. Bala Saidulu and K. L. Sebastian, *J. Chem. Phys.* **128**, 074708 (2008).
9. W.E. Paxton, A. Sen, T.E. Mallouk T. E., *Chem.–Eur. J.* **11**, 6462 (2005).
10. G. Rückner and R. Kapral, *Phys. Rev. Lett.* **98**, 150603 (2007).
11. R. Golestanian, T.B. Liverpool, and A. Ajdari, *New J. Phys.* **9**, 126 (2007).
12. J.L. Anderson, *Ann. Rev. Fluid Mech.* **21**, 61 (1989).
13. M.N. Popescu, S. Dietrich, and G. Oshanin, *J. Chem. Phys.* **130**, 194702 (2009).
14. F. Juelicher and J. Prost, *Eur. Phys. J. E* **29**, 27 (2009).
15. As noticed in the Introduction, in doing so one is bound by a number of assumptions which are either already present in the classical theory of phoresis or arise as a result of the mapping of such “active” surface particles into the framework of a theory developed to describe the case of inert particles immersed in a pre-defined, externally controlled concentration gradient. These assumptions are discussed in detail in Ref. [13]. For the purpose of the present work, we simply assume that such a mapping is possible and thus we subscribe to these assumptions.
16. A.B. Pawar and I. Kretzschmar, *Langmuir* **24**, 355 (2008); **25**, 9057 (2009).
17. T. Ohta and T. Ohkuma, *Phys. Rev. Lett.* **102**, 154101 (2009).
18. J. Happel and H. Brenner, *Low Reynolds number hydrodynamics* (Noordhoff International, Leyden, 1973), (**a**): Chaps. 4-26, 4-27, 4-30, and 4-31; (**b**): Chapt. 3-5, pp. 85-87.
19. A. Einstein, “On the Movement of Small Particles Suspended in a Stationary Liquid Demanded by the Molecular-Kinetic Theory of Heat” in *Investigations on the theory of the Brownian motion*, Ed. R. Fürth, transl. by A. D. Cowper (Dover, New York, 1956).
20. A. Ajdari and L. Bocquet, *Phys. Rev. Lett.* **96**, 186102 (2006).
21. Besides the translation described by  $\mathbf{V}$ , in the most general case a term accounting for a rigid-body rotation of the particle with angular velocity  $\mathbf{\Omega}$  should also be considered. However, this angular velocity turns out to be identically zero in most cases in which the particle has homogeneous surface properties [12, 22]. The azimuthal symmetry of our system and the additional assumption that the properties of the catalyst-covered surface are similar to those of the inert part (as far as the particle-solute effective interaction is concerned) ensures that we are dealing with such a case; therefore we disregard the rotation term here.
22. F.A. Morrison Jr., *J. Colloid Interface Sci.* **34**, 210 (1970).
23. G.R. Willmott, *Phys. Rev. E* **79**, 066309 (2009); **77**, 055302(R) (2008).
24. J.L. Anderson, *J. Colloid Interface Sci.* **105**, 45 (1985).
25. M.C. Fair and J.L. Anderson, *J. Colloid Interface Sci.* **127**, 388 (1989).
26. R. Golestanian, *Phys. Rev. Lett.* **102**, 188305 (2009).
27. M. Abramowitz and I.A. Stegun, *Handbook of Mathematical Functions with Formulas, Graphs, and Mathematical Tables* (Dover, New York, 1965), (**a**) p. 752; (**b**) p. 332; (**c**) p. 774; (**d**) p. 557.
28. H.F. Bauer, *J. Thermal Anal.* **35**, 1571 (1989).
29. W.R. Smythe, *Static and Dynamic Electricity* (McGraw-Hill, New York, 1968), Chaps. 5.21 - 5.28.
30. E.W. Hobson, *The Theory of Spherical and Ellipsoidal Harmonics* (Chelsea, New York, 1965), Chapt. II.
31. R.E. Collin, *Field Theory of Guided Waves* (McGraw-Hill, New York, 1960), pp. 553 - 570.
32. F. Pomer and J. Navasquillo, *J. Electrostatics* **22**, 309 (1989).
33. The numerical calculations have been performed using the software Mathematica (version 7.01), for which the Legendre function  $Q_\ell(x)$  for arguments  $x > 1$  or  $x \in \mathbb{C} \setminus \mathbb{R}$  is implemented as “the Legendre function Q of type 3” LegendreQ[ $\ell, 0, x, 3$ ].
34. H. Brenner, *Chem. Eng. Sci.* **19**, 703 (1964).